HPV18 Persistence Impairs both Basal and DNA Ligand-Mediated IFN-ß and IFN-ë1 Production Through Transcriptional Repression of Multiple Downstream Effectors of Pattern Recognition Receptor Signaling

Running Title: HPV18 persistence impairs IFN-ß and IFN-ë1 production

Silvia Albertini,[*] Irene Lo Cigno,[*] Federica Calati,[*] Marco De Andrea,[*,À] Cinzia Borgogna,[*] Valentina DellõOste,[À] Santo Landolfo,[À] and Marisa Gariglio[*]

[*]Department of Translational Medicine, Virology Unit, Novara Medical School, Italy; [À]Department of Public Health and Pediatric Sciences, Viral Pathogenesis Unit, Turin Medical School, Italy

Address correspondence to Marisa Gariglio (MG)

Phone number: ++39 0321 660649

Fax number: ++39 0321 620421

E-mail address: marisa.gariglio@med.uniupo.it

S.A. and I.L.C. contributed equally to this work.

Abstract

While it is clear that high-risk human papillomaviruses (hrHPVs) can selectively infect keratinocytes and persist in the host, it still remains to be unequivocally determined whether they can escape antiviral innate immunity by interfering with pattern recognition receptor (PRR) signaling. Here, we have assessed the innate immune response in monolayer and organotypic raft cultures of NIKS cells harboring multiple copies of episomal HPV18 (named NIKSmcHPV18), which fully recapitulate the persistent state of infection. We show for the first time that NIKSmcHPV18, as well as HeLa cells (a cervical carcinoma-derived cell line harboring integrated HPV18 DNA) display marked downregulation of several PRRs as well as other PRR downstream effectors such as the adaptor protein STING and the transcription factors IRF1 and IRF7. Importantly, we provide evidence that downregulation of STING, cGAS, and RIG-I mRNA levels occurs at the transcriptional level through a novel epigenetic silencing mechanism as documented by the accumulation of repressive heterochromatin markers seen at the promoter region of these genes. Furthermore, stimulation of NIKSmcHPV18 cells with salmon sperm DNA (SS DNA) or poly(dA:dT), two potent inducers of PRR signaling, only partially restored PRR protein expression. Accordingly, the production of both IFN-ϐ and IFN-ϙ1 was significantly reduced in comparison to parental NIKS cells, indicating that HPV18 exerts its immunosuppressive activity through downregulation of PRR signaling. Altogether, our findings indicate that hrHPV have evolved broad-spectrum mechanisms that allow simultaneous depletion of multiple effectors of the innate immunity network, thereby creating an unreactive cellular milieu suitable for viral persistence.

Introduction

Human papillomaviruses (HPVs) comprise a large family of sexually transmitted DNA viruses, which can cause both benign and malignant lesions in humans (1-4, https://pave.niaid.nih.gov/). Although it has been known for quite some time that HPVs are able to evade the innate immune response and persist in the host, the molecular mechanisms regulating these critical events have only recently begun to emerge and still remain largely uncharacterized (5-7). Thus, gaining mechanistic insights into the immune escape by HPVs would allow us to better understand how these viruses can favor cancer progression.

Among the HPV family members, high-risk HPV (hrHPV) genotypes, especially HPV16 and 18, selectively infect human keratinocytes (KCs) in stratified epithelia of mucosa leading to epithelial hyperplasia, which can subsequently progress to cancer at different anatomical sites, such as the anogenital tract and oropharynx (8, 9). Since undifferentiated KCs express several pattern recognition receptors (PRRs), which are able to sense viral pathogens and promote the innate immune response (10-12), it is highly likely that hrHPVs have developed effective strategies to evade the innate immunity by inhibiting PRR downstream signaling (13-16). In support of this hypothesis, a recent report by Laura Lau and co-workers has shown that E6 and E7 deregulation in transformed KCs antagonizes the cGAS-STING pathway. In particular, E7 was found to directly bind STING, thereby acting as a specific antagonist of the DNA-activated antiviral response (17). In addition, others have shown that E6 or E7 protein from hrHPV genotypes inhibits the transcriptional activity of IRF family members (18-22). However, there are several caveats affecting the interpretation and generalizability of the aforementioned findings such as the heterogeneity of the cell models employed (e.g. cells of different origin such as epithelial cells and fibroblasts, cells overexpressing only E6 and E7, cells transfected with

episomal viral genomes, or transformed cells harboring multiple copies of the integrated viral genome) and the multiplicity of stimuli used to test host innate immunity. Thus, while it is clear that hrHPVs can selectively infect basal KCs and persist in the host, it still remains to be unequivocally determined how, in HPV-infected KCs, the physical status of the virus, different cell-type specific microenvironments, or different stimuli may affect the host innate antiviral response. Furthermore, whether HPV interferes with the expression of PRRs in HPV episome-containing KCs still remains an open question. Thus, there is a significant gap in our knowledge of the pathogenic mechanisms of hrHPV in human KCs.

The interferon (IFN) system constitutes the first line of defense against viruses in mammals. IFNs are categorized into three groups: type I [alpha/beta IFN (IFN-α/β)], type II [gamma IFN (IFN-γ)], and type III [lambda IFN (IFN-λ)]. Among them, IFN-λ is the most recently described group of small helical cytokines capable of inducing an antiviral state in responsive cells (23-26). Although type I IFNs act in most mammalian cell types, type III IFNs appear to primarily target mucosal surfaces, particularly epithelial cells of the intestine, liver, lung, and presumably skin (27-29).

In this study, we have deliberately chosen as our cell model the near-diploid, spontaneously immortalized human keratinocyte cell line (NIKS), which retains a normal response to contact inhibition, supports the full productive HPV life cycle, and provides an isogenic cell background where to study virus-host interactions (30, 31). Using this cell model, which recapitulates the full viral life cycle of HPV, we show that NIKS cells harboring multiple copies of episomal HPV18 genomes fail to produce both type I and III IFNs not only under differentiating conditions, but also following exposure to either salmon sperm DNA (SS DNA) or poly(dA:dT), two potent inducers of PRR signaling (32-35). Lastly, we report the existence of

multiple evasion mechanisms relying on HPV18-mediated transcriptional inhibition of key components of the cGAS-STING and RIG-I DNA-sensing pathways.

Overall, our findings provide novel insights into HPV18 immune escape mechanisms in human KCs with possible implications in cervical carcinogenesis.

Materials and Methods

Cell culture, transfection, and treatments.

NIKS cells (Stratatech Corporation) were cultured in the presence of J2 3T3 fibroblast feeders as previously described (36). HeLa cells were grown in DMEM (Sigma-Aldrich) supplemented with 10% FBS (Sigma-Aldrich). HPV18 minicircle genome was produced as previously described (37). Briefly, for construction of minicircle viral genomes, a BglII site was introduced into the HPV18 genome after nucleotide 7,473 and the minicircle vector pMC.BESPX was subcloned into this site. For the production of minicircles, the *Escherichia coli* strain ZYCY10P3S2T was transformed and grown in TB medium until an optical density at 600 nm (OD600) of 4-5 was reached. An equal volume of induction mix (0.04 N NaOH and 0.02% L-arabinose in LB broth) was added to induce recombination, and the culture was incubated for an additional 5 h at 32°C. Subsequently, plasmid DNA was extracted from bacteria and gel purified to obtain only the covalently closed circular DNA (cccDNA) form of the viral genome.

NIKSmcHPV18 cells were obtained by nucleofection of NIKS cells with Nucleofector II Amaxa (Biosystems) with 2 µg of HPV18 minicircles according to the manufacturerôs instructions, grown as pooled cells, and used from passages 20 to 30. Organotypic raft cultures were generated as previously described in Wilson and Laimins, 2005 (38). Briefly, organotypic cultures were grown in specialized culture chambers on a collagen base, formed by mixing normal human neonatal fibroblast with Collagen I Rat Tail (Sigma) in Hamôs F-12 medium containing 10% FBS and penicillin/streptomycin. NIKS cells were plated on the collagen base and after 15 days, raft cultures were harvested and fixed in 10% buffered formalin, embedded in paraffin, and cut into 5-ε m sections for immunostaining analysis.

Poly(dA:dT) (1.25 εg/ml) and sheared salmon sperm DNA (SS DNA) (1.25 εg/ml) (InvivoGen) were transfected into the cells using Lipofectamine 3000 according to the manufacturerôs instructions (Thermo Fisher Scientific). Cells were treated with carbonyl cyanide m-chlorophenylhydrazone (CCCP; Sigma-Aldrich) at 10 εM concentration or DMSO for 30 min and then transfected for 24 h with poly(dA:dT). MG132 (Sigma-Aldrich) was used at 30 εM concentration for 8 h.

Immunoblotting and native page.

Whole-cell protein extracts were prepared and subjected to immunoblot analysis as previously described (39). The following antibodies were used: rabbit polyclonal antibodies anti-cGAS (HPA031700; Sigma-Aldrich, diluted 1:500), RIG-I (06-1040; Merck Millipore, diluted 1:10000), IFI16 (C-terminal, diluted 1:1000), IRF7 (sc-9083; Santa Cruz, diluted 1:200), IRF3 (sc-9082; Santa Cruz, diluted 1:500), rabbit monoclonal antibodies anti-IRF1 (8478; Cell Signaling, diluted 1:250), pSTAT1 (9167; Cell Signaling, diluted 1:1000), or mouse monoclonal antibodies (MAb) anti-STING (MAB7169; R&D Systems, 1:1500), MAVS (sc-166583; Santa Cruz, diluted 1:200), STAT1 (610186; BD Biosciences, diluted 1:1000); MAb against Ŭ-tubulin (39527; Active Motif, diluted 1:4000) were used as a control for protein loading. Immunocomplexes were detected using sheep anti-mouse or donkey anti-rabbit immunoglobulin antibodies conjugated to horseradish peroxidase (HRP) (GE Healthcare Europe GmbH) and visualized by enhanced chemiluminescence (Super Signal West Pico; Thermo Fisher Scientific). Native polyacrylamide gel electrophoresis (PAGE) was performed using ReadyGels (7.5%; Bio-Rad) as described previously (40). In brief, the gel was pre-run with 25 mM Tris base and 192 mM glycine, pH 8.4, with 1% deoxycholate (DOC) in the cathode chamber for 30 min at 40 mA.

Samples in native sample buffer (20 εg protein, 62.5 mM Tris-HCl [pH 6.8], 10% glycerol, and 1% DOC) were size fractionated by electrophoresis for 60 min at 25 mA and transferred to nitrocellulose membranes for western blot analysis. Images were acquired, and densitometry of the bands was performed using Quantity One software (version 4.6.9; Bio-Rad Laboratories Srl). Densitometry values were normalized using the corresponding loading controls.

Quantitative nucleic acid analysis.

Real-time quantitative reverse transcription (qRT)-PCR analysis was performed on a CFX96^{tm} Real Time System (Bio-Rad Laboratories Srl). Total RNA was extracted using TRI Reagent (Sigma-Aldrich), and 1 εg was retrotranscribed using iScript cDNA Synthesis kit (Bio-Rad Laboratories Srl). Reverse-transcribed cDNAs were amplified in duplicate using SsoAdvanced Universal SYBR green Supermix (Bio-Rad Laboratories Srl) for viral genes, as well as cellular genes. The glucuronidase beta (GUSB) housekeeping gene was used to normalize for variations in cDNA levels.

Total cellular DNA was isolated with QIAamp DNA Mini kit (Qiagen). A 600 ng DNA sample was digested with DpnI to remove the unreplicated input DNA. After digestion, 40 ng were analyzed by quantitative PCR (qPCR) using 500 nM primers and SsoAdvanced Universal SYBR green Supermix (Bio-Rad Laboratories Srl). The reaction conditions consisted of a 30 s 95°C enzyme activation cycle, 40 cycles of 10 s denaturation at 95°C, and 10 s annealing at 60°C. Copy number analysis was completed by comparing the unknown samples to standard curves of linearized HPV18 DNA. The glyceraldehyde 3-phosphate dehydrogenase (GAPDH) DNA copy number was used as an endogenous control. The specificity of the L2 primers was tested in nontransfected cells where no amplification occurred. The primer sequences are

detailed in Supplemental Table 1.

ELISA and ELISA-based transcription factor assay.

The cytokines secreted in culture supernatants were analyzed using Single Analyte Human ELISA kits for IFN-β (41410; VeriKine™ Human IFN Beta ELISA KIT, PBL Assay Science) and IFN-λ1 (DY7246; DuoSet ELISA Human IL-29/IFN-λ1 R&D Systems) according to the manufacturer's instructions. All absorbance readings were measured at 450 nM using a Victor X4 Multilabel Plate Reader (Perkin Elmer).

Nuclear extracts were prepared using NE-PER Nuclear and Cytoplasmic Extraction Reagent (78883; Thermo Fisher Scientific) according to the manufacturer's instructions. IRFs binding activity to IFN-β and λ1 enhancers, was measured by Universal Transcription Factor Assay Colorimetric kit (70501; Merck Millipore) according to the manufacturer's instructions. In brief, 200 ng biotin-labeled oligonucleotides containing the consensus sequence for the specific transcription factor under study were mixed with nuclear extract into each well of a streptavidin-coated microtiter plate. The bound transcription factor was detected with a specific primary antibody: anti-IRF1 (sc-497X; Santa Cruz, diluted 1:400), anti-IRF3 (sc-9082X; Santa Cruz, diluted 1:400), anti-IRF7 (sc-9083X; Santa Cruz, diluted 1:200). An HRP-conjugated antibody was then used for detection with TMB substrate. The intensity of the reaction was measured at 450nM using a Victor X4 Multilabel Plate Reader. The biotinylated oligonucleotides used were: IFN-β enhancer probe sense 5'- biotin ATGACATAGGAAAACTGAAAGGGAGAAGTGAAAGTGGGAAATCCTCTG- 3' and IFN-β enhancer probe antisense 5'- CAGAGGAATTTCCCACTTTCACTTCTCCCTTTCAGTTTTCCTATGTCAT- 3', IFN-λ1

207 enhancer probe sense 5ô- biotin
208 AGGGAGTTCTAAGGATTTCAGTTTCTCTTTCCTTCTTGATGCAGCTCCCA- 3ô and IFN-
209 ά1 enhancer probe antisense 5ô-
210 TGGGAGCTGCATCAAGAAGGAAAGAGAAACTGAAATCCTTAGAACTCCCT-3ô
211
212 *Southern blot analysis.*
213 Southern blot analysis was performed as described previously (36). In brief, genomic
214 DNA (10 εg) was digested with DpnI to remove any residual input DNA and with HindIII,
215 which has no restriction site in HPV18, or EcoRI, which has two restriction sites in HPV18
216 minicircles. The digested DNA was the separated on a 0.8% agarose gel, blotted, and hybridized
217 with an HPV18 genome sequence-specific probe labeled with [Ŭ-^{32}P]dCTP using Ready-To-Go
218 DNA Labeling. The results were quantitated using a Personal Molecular Imager (PM) System
219 (Bio-Rad Laboratories Srl) equipped with Quantity One software.
220
221 *FISH, immunofluorescence and immunohistochemistry analysis.*
222 Five εm sections obtained from NIKSmcHPV18 organotypic raft cultures were processed
223 for immunofluorescent analysis and DNA-fluorescent in situ hybridization (FISH), as previously
224 described (41). The following antibodies were used: anti-MCM7 (CDC47, MS-862-P; Neo
225 Markers, diluted 1:200), anti-p16 (clone E6H4) was obtained from Ventana Medical System,
226 anti-HPV Ŭ-genus E4 protein (namely PanHPVE4). FISH probe was generated by using a Biotin
227 Nick Translation Mix (Roche Diagnostics SpA) according to the manufacturerôs protocol with
228 the HPV18 minicircle genome as a template. Images were acquired using a digital scanner
229 (Pannoramic MIDI; 3D Histech Kft.). For the assessment of histological features, the slides

analyzed by HPV18 E4, MCM7 or HPV18 DNA were disassembled and stained with hematoxylin and eosin (H&E).

ChIP assay.

ChIP assays were performed as previously described (36). Immunoprecipitation was performed with 3 µg of unmodified histone H3 (06-755), dimethyl-histone H3 (Lys4; 07-030) and dimethyl-histone H3 (Lys9; 07-441) antibodies, all purchased from Merck Millipore (Merck Millipore SpA). Threshold cycle (CT) values for the samples were equated to input CT values to give percentages of input for comparison and these were normalized to the enrichment level of unmodified histone H3 for each cell line. The primers used to amplify STING, cGAS, and RIG-I promoters are detailed in Supplemental Table 1.

Statistical analysis.

All statistical tests were performed using Graph-Pad Prism version 5.00 for Windows (GraphPad Software). The data are presented as mean ± standard deviation (SD). For comparisons consisting of two groups, means were compared using two tailed Studentôs t tests; for comparisons consisting of three groups, means were compared using one-way or two-way analysis of variance (ANOVA) with Bonferroniôs post test. Differences were considered statistically significant at a P value of < 0.05.

Results

HPV18 replication fails to induce antiviral or pro-inflammatory cytokines and inhibits DNA ligand-mediated production of type I and III IFNs.

First, we asked whether HPV18 replication *per se* would induce an antiviral response in KCs. For this purpose, we generated a human KC cell line, named NIKSminicircleHPV18, abbreviated as NIKSmcHPV18, stably harboring high viral load of HPV18 episomal genomes (37, 42). These cells were cultured as pooled cells and used throughout the study at passages between 20 and 30. NIKSmcHPV18 cells maintained episomal HPV18, as assessed by the representative Southern blot analysis shown in Fig. 1A. The slower migrating bands seen in the DNA sample digested with the non-cutter restriction enzyme Hind III indicate the presence of concatamers (Fig. 1A). As expected for episomal harboring cells, NIKSmcHPV18 cells formed low squamous intraepithelial lesions (L-SILs) in organotypic raft cultures, as determined by enhanced expression levels of the cellular proliferation marker minichromosome mainteinance-7 (MCM7) in the suprabasal layers where E4 expression was also well evident (Fig. 1B) (43). Viral load was measured by qPCR of total genomic DNA at various passages along with the quantification of viral transcription from total RNA extracts. We measured mRNA expression levels of E6, E7, and E2 oncogenes, with the latter being a specific marker of episome-derived transcription. As shown in Fig. 1C, the viral load ranged from 200 to 60 copies *per* cell. Furthermore, cells cultured from passage 20 expressed much higher levels of E6 and E7 mRNA than those of E2 (Fig. 1D). Consistent with this viral mRNA expression pattern, cells were found negative for p53 protein expression (data not shown). Despite the variations observed in viral load and viral mRNA expression levels, both Southern blotting pattern and L-SIL phenotype remained unchanged between passages 20 and 30 and the results described onwards were

276 performed at different passages with reproducible results.

277 Next, we measured mRNA expression levels of both type I and III IFN genes along with
278 those of some pro-inflammatory cytokines in both NIKSmcHPV18 and NIKS cells. All IFN
279 mRNAs, with the exception of IFN-ŭ, were significantly downregulated in NIKSmcHPV18 cells
280 when compared to parental cells (Fig. 2A). Intriguingly, we observed a significant upregulation
281 of the IL-6 gene product, while the other cytokines were only marginally affected.

282 To obtain a cell model that would more closely recapitulate the natural replication of
283 HPV, we generated organotypic raft cultures using both NIKS and NIKSmcHPV18 cells and
284 measured the mRNA expression levels of the same panel of genes described above. As shown in
285 Fig. 2B, both type I and III IFN mRNA levels were significantly downregulated in
286 NIKSmcHPV18 cells when compared to those of parental cells, indicating that HPV-mediated
287 escape from the immune response correlates with inhibition of IFN gene expression. IL-18
288 mRNA expression levels were also significantly downregulated, whereas those of IL-6 and IL-8
289 were significantly upregulated.

290 We next asked whether NIKSmcHPV18 cells were still able to react to exogenous DNA
291 ligands in terms of type I and III IFN production. Since the physical status of the virus, episomal
292 or integrated, may generate variability in the innate immune response of epithelial cells, we also
293 included in our analysis HeLa cells harboring an integrated HPV18 DNA (44, 45). Cells cultured
294 between 20 and 30 passages were transfected with SS DNA or the viral dsDNA analogue
295 poly(dA:dT), and then total RNAs were isolated from cells at the 12 h time point, while their
296 supernatants were collected after 24 h of treatment to allow enough time for lymphokines to
297 accumulate in the medium. Transfection of NIKS with either poly(dA:dT) or SS DNA increased
298 mRNA expression levels of all IFNs tested, with IFN-ƃ and IFN-ə1 being the highest induced

299 genes (Fig. 3A); in all cases, SS DNA was a less potent inducer than poly(dA:dT). Remarkably,
300 in both NIKSmcHPV18 and HeLa cells, DNA ligand-mediated induction of all IFN genes tested
301 was dramatically reduced compared to NIKS cells (Fig. 3A).

302 Next, we assessed the extent of IFN-ϐ and IFN-ə1 production at the protein level by
303 ELISA. Consistent with the mRNA levels, IFN-ϐ production in poly(dA:dT)- or SSDNA-
304 transfected NIKSmcHPV18 cells was markedly downregulated compared to control cells (i.e.
305 80% and 83 reduction, respectively), while it was barely detectable in HeLa cells (Fig. 3B).
306 Likewise, DNA ligand-mediated IFN-ə1 production was significantly inhibited in either cell
307 types compared to control cells [e.g. 68% and 46% reduction in NIKSmcHPV18 cells, and 89
308 and 98% in HeLa cells transfected with either poly(dA:dT) or SS DNA, respectively] .

309 Lastly, in good agreement with previous findings showing hyperactivation of NF-əB
310 transcriptional activity in KCs overexpressing hrHPVE6 and E7 (46-48), we found that
311 NIKSmcHPV18 and HeLa cells transfected with DNA ligands displayed increased expression of
312 IL-6, an NF-əB downstream target gene, at both the mRNA and protein levels (Fig. 3A and C,
313 respectively) compared to control cells.

314 Altogether, these findings clearly indicate that: i) episomal HPV18 does not induce an
315 antiviral innate immune response; ii) KCs carrying episomal HPV18 as well as HeLa cells poorly
316 respond to exogenous DNA ligands in terms of both type I and III IFN production compared to
317 parental cells; and iii) the HPV18 inhibitory activity does not seem to affect NF-əB function.

318

319 *Dysregulation of the innate immune response in HPV18-positive keratinocytes is characterized*
320 *by specific alterations in antiviral innate signaling pathways.*

321 To gain more insights into the molecular mechanisms of HPV18-mediated regulation of

type I and III IFN expression levels in NIKSmcHPV18 cells and HeLa cells, we measured by Western blot protein levels of various PRRs (i.e. cGAS, RIG-I, and IFI16), the adaptor molecules STING and MAVS, as well as the transcription factors IRF1, 3 and 7. Fig. 4A illustrates the schematic representation of the pathways involved in the innate immune response to exogenous DNA. cGAS, STING, RIG-I, and IFI16 were all very low in both untreated NIKSmcHPV18 and HeLa cells compared to NIKS cells, while MAVS did not vary significantly (Fig. 4B and C). When we transfected these cells with poly(dA:dT) for 24 h, we observed a slight increase in cGAS expression in NIKS cells but not in NIKSmcHPV18 and HeLa cells. IFI16 displayed a dual expression pattern. While it was downregulated in poly(dA:dT)-transfected NIKS cells, it was significantly upregulated in both NIKSmcHPV18 and HeLa cells similarly treated. RIG-I induction by poly(dA:dT) was observed in both KCs carrying episomal HPV18 and NIKS. As expected, STING expression levels were reduced after poly(dA:dT) transfection in NIKS cells, while they remained barely detectable in HPV-infected cells (49).

A recent report has shown that E7 is a potent and specific inhibitor of the cGAS-STING pathway, thereby hampering type I IFN production by DNA ligands in HeLa cells (17). While not reported in that study, here we found that both STING and cGAS are barely detectable or absent in NIKSmcHPV18 and HeLa cells (Fig. 4B and C), suggesting that one of the possible mechanism by which HPV18 keeps antiviral factors in check is through downregulation of STING expression.

When we measured the expression of IRF1, 7, and 3 proteins (Fig. 4D to G), we made the following observations: i) IRF1, which was barely detectable in all untreated cells, was strongly induced in both poly(dA:dT)-transfected NIKS and HeLa cells but not NIKSmcHPV18 cells, reaching a peak in both cases at the 24 h time point; ii) IRF7 expression, which was very low in

untreated NIKS cells, was strongly induced upon poly(dA:dT) transfection with a peak at the 12 h time point. In contrast, IRF7 induction by poly(dA:dT) was completely ablated in HeLa cells and strongly delayed in NIKSmcHPV18, where it became evident only at the 24 h time point; iii) IRF3 protein expression, which was readily detectable in all untreated cells, did not vary following poly(dA:dT) transfection (Fig. 4F and G). We also observed IRF3 dimerization after poly(dA:dT) transfection in all cell lines, although in KCs harboring episomal HPV18 dimer formation was slower compared to NIKS cells (Fig. 4H and I).

Thus, it seems that the defects in type I and III IFN production observed in NIKSmcHPV18 cells after poly(dA:dT) transfection may be ascribed to multiple abnormalities in antiviral innate signaling pathways. In particular, the reduced availability of cGAS, STING, RIG-I, and IFI16 in HPV-infected cells, together with the lack of induction of IRF1 and IRF7, might provide the rationale for HPV18 immune evasion after DNA ligand stimulation.

The RIG-I-MAVS pathway is restored upon poly(dA:dT) transfection in HPV18-positive cells, while the cGAS-STING pathway remains inhibited.

Since poly(dA:dT) transfection was shown to be able to induce IFN-ϐ even in cells void of cGAS and STING (50), we asked whether downregulation of the polymerase III-RIG-I-MAVS signaling pathway activity by HPV could partly explain our observation that this stimulus failed to induce both type I and III IFN production in NIKSmcHPV18 and HeLa cells, but not NIKS cells. To this end, we first looked at RIG-I mRNA expression levels in either mock or poly(dA:dT)-transfected cells at different time points. Consistent with our previous data (Fig. 4B and C), basal RIG-I mRNA levels were reduced in both NIKSmcHPV18 and HeLa cells compared to NIKS cells (20% and 98%, respectively) (Fig. 5A). Upon poly(dA:dT) transfection,

368 RIG-I mRNA was quickly induced in NIKS cells at 3 h, reaching a peak at 12 h, while in HPV-
369 positive cells RIG-I started to increase only at the 6 h time point, albeit to a lesser extent
370 throughout the time course. The same delayed kinetics was observed at the protein level, where
371 the protein became more evident after 6 h in HPV-positive cells, while it was induced at the 3 h
372 time point in parental cells (Fig. 5B). This delay in RIG-I induction in HPV-positive cells might
373 also explain the delayed formation of IRF3 homodimers occurring in these cells after
374 poly(dA:dT) stimulation (Fig. 4H and I). When we measured IFNs in the supernatants, we found
375 them quickly released in NIKS cellsð IFN-ß at 6 h and IFN-α1 at 12 hð while in HPV-positive
376 cells they were both induced at 12 and 24 h, respectively (Fig. 5C).
377 Next, we asked whether the RIG-I-MAVS pathway mediated IFN induction in response
378 to poly(dA:dT) transfection. To this end, we inhibited MAVS with the protonophore carbonyl
379 cyanide m-chlorophenylhydrazone (CCCP), which is capable of ablating RLR signaling through
380 disruption of mitochondrial integrity (51). Consistent with a previous report (52), CCCP-treated
381 NIKS cells remained viable and metabolically active throughout the 2-day-long experiment (data
382 not shown). As expected, poly(dA:dT)-induced IFN-ß and IFN-α1 production was markedly
383 reduced in both NIKSmcHPV18 and HeLa cells compared to that of NIKS cells (Fig. 5C and D).
384 CCCP treatment of NIKS cells led to a 2.5-fold decrease in both IFN-ß and IFN-α1 production,
385 which nevertheless remained much higher than DMSO-treated NIKSmcHPV18 and HeLa cells
386 (Fig. 5D). Likewise, CCCP treatment of poly(dA:dT)-transfected NIKSmcHPV18 cells
387 downregulated IFN-ß and IFN-α1 of about 1.5-fold and 1.8-fold, respectively compared to
388 DMSO-treated NIKSmcHPV18 cells. IFN-α1 production was also reduced in HeLa cells of about
389 2.6-fold compared to DMSO-treated cells, while levels of IFN-ß remained constantly low. Thus,
390 in HPV-positive cells, where the STING pathway is apparently turned off, the amount of IFN

391 produced upon poly(dA:dT) treatment seems to be mainly mediated by the RIG-I-MAVS
392 pathway. Furthermore, the delayed kinetics of IFN production in these cells might be due to the
393 unavailability of RIG-I under basal conditions. Lastly, reduced RIG-I mRNA levels in untreated
394 HPV-positive cells suggests that HPV acts as a RIG-I transcriptional repressor able to dampen
395 the innate antiviral response during persistent infection. Likewise, basal mRNA levels of both
396 cGAS and STING were significantly lower than those seen in parental cells [i.e. 60% and 90%
397 for cGAS and STING in NIKSmcHPV18 cells, and 64% and 65% in HeLa cells, respectively
398 (Fig. S1)].

399 Recent evidence indicates that STING transcriptional regulation is mediated by STAT1
400 binding (53, 54). In addition, STAT1 transcriptional activity was markedly inhibited in hrHPV-
401 infected KCs (55), thus providing a possible mechanistic framework by which HPVs
402 downregulate STING in host cells. We therefore assessed STAT1 expression at both the mRNA
403 and protein level at baseline or after poly(dA:dT) transfection as described above. In good
404 agreement with previous findings, STAT1 mRNA basal levels in HPV-positive cells were
405 reduced by 52% in NIKSmcHPV18 and 92% in HeLa compared to NIKS cells. Furthermore,
406 STAT1 expression was induced in all cell lines following poly(dA:dT) transfection, albeit to a
407 much lesser extent in HPV-positive cellsð approximately 80% less than parental cells at the 12 h
408 time point (Fig. 6A). Consistent with the mRNA induction kinetics, both total and
409 phosphorylated STAT1 protein levels increased upon poly(dA:dT) transfection in HPV-positive
410 cells with a delay of 6 and 12 h in NIKSmcHPV18 and HeLa cells, respectively (Fig. 6B).

411 To confirm that the downregulation of these proteins by HPV18 was occurring at the
412 transcriptional level, we treated cells with the proteasome inhibitor MG132 for 8 h, and then
413 assessed protein levels of various PRRs and adaptor molecules as described above. Even though

414 the drug induced accumulation of ubiquitylated proteins, it did not promote any accumulation of
415 the proteins analyzed (Fig. 6C).

416 Thus, our results indicate that viral immune escape in HPV-positive cells is due to
417 constitutive downregulation of at least two important cytoplasmic PRRs, cGAS and RIG-I, and
418 the adaptor protein STING. Furthermore, low levels of STAT1 factor may explain why STING
419 basal expression is reduced in HPV-positive cells.

420

421 *HPV18 promotes heterochromatin association with the promoter region of STING, cGAS, and*
422 *RIG-I genes*.

423 Broad regulation of the transcriptional competence of host cell chromatin has been
424 previously reported in HPV-infected cells (56-59). To verify whether the transcriptional
425 inhibition of the cGAS, STING, and RIG-I genes observed in HPV-positive cells could also
426 reflect changes in chromatin structure, we examined histone associations whit the promoter
427 region of the above mentioned genes in HPV-positive *vs.* parental cells by ChIP assay. For this
428 experiment, we chose dimethylation of histone H3 lysine 4 (H3K4me2) as a mark of actively
429 transcribing genes, and dimethylation of histone H3 lysine 9 (H3K9me2) as a mark of
430 heterochromatin. We then performed ChIP assay using lysates from formaldehyde-fixed
431 NIKSmcHPV18, HeLa, and NIKS cells, and two sets of PCR primers that could specifically
432 amplify the promoter regions of the STING, cGAS, and RIG-I genes. The first primer set
433 encompassed the promoter region where the putative STAT1 binding site is located (segment 1),
434 while the second set was directed to a flanking region always within the promoter that included
435 the transcription start site (TSS), which, in the case of cGAS, also included the putative
436 interferon-sensitive response element (ISRE) binding site (segment 2) (Fig. 7A). As shown in

Fig. 7B, HPV18 had little or no effect on the association of H3K4me2 (active chromatin) with either segment 1 or 2 in all three promoters. In contrast, we observed a significant increase in H3K9me2 (repressive chromatin) bound to the two segments in all promoters from lysates of HPV-positive *vs.* NIKS cells. Interestingly, dimethylated H3K9me2 binding levels to the three promoter regions in NIKSmcHPV18 were 5- to 15-fold higher than those seen in NIKS cells for both segments. In HeLa cells, we detected even higher H3K9me2 binding levels to segments 1 and 2 of the same promoter regions than those observed in NIKSmcHPV18 cells. The levels of H3K9me2 and H3K4me2 bound to gene segments located far away from the promoter region were comparable in all three cell lines as well as in the GAPDH promoter region (Fig. S2). Thus, HPV18 represses STING, cGAS, and RIG-I gene expression by promoting heterochromatin association with their promoter regions.

The binding activity of IRF1 and 7 but not IRF3 to the IFN enhancer is reduced in HPV-infected cells.

Since IRF family members displayed different temporal protein profiles in HPV-positive *vs.* parental cells upon DNA ligand stimulation (Fig. 4D and E), and we detected concomitant induction of IRF3 homodimer formation (Fig. 4H and I), albeit significantly delayed in HPV-expressing cells, we sought to determine whether IRF species were transcriptionally active in these cells. For this purpose, we performed a sensitive quantitative ELISA-based assay using a biotin-labeled probe that spanned the tandem IRF binding sites present in either the IFN-β or IFN-α_1 enhancer (Fig. 8A). Since identical results were obtained with both probes, only the set of panels for IFN-β is shown in Fig. 8B. IRF1, 3, and 7 all bound very efficiently to the immobilized probes in poly(dA:dT)-transfected NIKS cells, and their binding kinetics mirrored

the changes in protein expression. Specifically, IRF1 binding activity was readily induced in both poly(dA:dT)-transfected NIKS and HeLa cells (Fig. 8B), in a fashion consistent with the changes in protein expression (Fig. 4D and E). In contrast, NIKSmcHPV18 cells displayed low basal IRF1 binding activity, which remained basically unchanged throughout the entire time course following poly(dA:dT) transfection, in good agreement with the protein expression kinetics shown in Fig. 4D and E. On the other hand, induction of IRF3 binding activity by poly(dA:dT) was readily detectable at the 3 h time point and did not differ among cell lines (Fig. 8B). Lastly, induction of IRF7 binding activity was observed only after 12 h of poly(dA:dT) transfection of NIKS cells, whereas it was inhibited in both NIKSmcHPV18 and HeLa cells similarly treated, mirroring the protein expression kinetics shown in Fig. 4D and E. Thus, it appears that HPV can interfere with IRF DNA binding activity following DNA ligand-stimulation in a cell type-specific fashion, thereby hampering the innate immune response in these cells.

Discussion

Escape from innate immune surveillance appears to be the hallmark of HPV infections (6, 7, 60). Although some mechanisms of immune evasion by HPVs, especially HPV16, have been previously characterized, they were mostly based on results obtained from either KCs overexpressing only E6 and E7 or non-epithelial cells, thereby hampering data interpretation (17-21).

Here, in order to better recapitulate the HPV impact on its natural target cells (i.e. KCs), we have assessed the innate immune response in NIKSmcHPV18 cells, which are KCs carrying high numbers of episomal viral genome copies. These cells were used at passages between 20 and 30, when the E6 and E7 transcripts were higher than those of E2, an expression pattern typical of persistent HPV infection. For comparison, we also included HeLa cells, which are cervical carcinoma-derived transformed cells harboring integrated HPV18 genomic DNA characterized by deregulated overexpression of E6 and E7 oncogenes (44,45). We then used these cells to determine how persistent infection with HPV would affect their response to exogenous DNA.

Our findings demonstrate that KCs can maintain high copy number of episomal viral DNA without triggering an antiviral response because multiple points of the molecular pathways involved in the induction of both type I and III IFNs are being inhibited. In this regard, we failed to detect any IFN production in KCs grown either in monolayer or under differentiating conditions using organotypic raft cultures. Consistent with other reports, the NF-əB dependent gene IL-6 was upregulated at higher levels in HPV-positive cells compared to parental cells, indicating that the NF-əB pathway was functionally active in KCs carrying episomal HPV18 as well as HeLa (46-48).

When we stimulated NIKSmcHPV18 with DNA ligands, we found that induction of both IFN-β and IFN-λ1 were significantly reduced compared to parental cells. Remarkably, cGAS, STING, RIG-I and IFI16 proteins were all poorly expressed or almost undetectable in NIKSmcHPV18 cells when compared to parental NIKS cells. Their suppression mainly occurred at the mRNA rather than the protein level. The observed increase in repressive heterochromatin markers at the promoter region of STING, cGAS, and RIG-I genes argues in favor of epigenetic silencing of these genes as a mechanism to stably repress key components of the innate antiviral response against DNA viruses.

Thus, altogether, our findings support a model whereby reduced expression of PRRs in HPV-positive cells, along with that of the adaptor protein STING (61), which bridges most DNA receptors to downstream signaling events, create an unreactive cellular milieu suitable for viral persistence, replication and tumorigenesis (Fig. 9). In support of this model, human osteosarcoma U2OS cells, which are highly permissive to HPV replication, display a series of defects in innate immunity, including the absence of cGAS and STING proteins (37, 42, 62, and unpublished personal data). As all these proteins are considered to be IFN-stimulated genes (ISGs), our findings are consistent with previous reports demonstrating that hrHPV genotypes inhibit a number of ISGs at the transcriptional level (22, 58, 63-65). However, these mechanisms differ from the evasion strategies reported for many other viruses that usually target PRRs and downstream molecules through post-translational modifications leading to increased protein degradation and temporary shutdown of the signaling cascade (66-69). These events usually take place at the early stages of infection. This discrepancy can be easily explained by the fact that we are dealing with a virus that displays an unusual life cycle, as it does not cause lytic infection, but rather has evolved strategies to remain inside the cells for a very long time, can replicate without

being recognized by innate sensors, and eventually promotes tumorigenesis (70). Thus, in our model of viral persistence, it is not unexpected that we found alternative strategies used by these viruses to keep the guardians in a prolonged inactive state. This inhibitory activity seems to be irreversible in the case of the cGAS-STING pathway, as we did not find any recovery of these proteins even after treatment with exogenous DNA, while RIG-I protein expression was induced in response to poly(dA:dT) transfection and likely mediated the residual IFN production observed in both HPV-positive cells (Fig. 9). Indeed, when we exposed poly(dA:dT) transfected HPV-positive cells to the protonophore CCCP, a known disruptor of RIG-I-MAVS signaling (51,52), both type I and III IFN levels in the supernatants were dramatically reduced. Furthermore, RIG-I upregulation was delayed in HPV-positive cells and accompanied by the induction of IFNs, indicating that this pathway could be restored and was responsible for the delayed antiviral response. Intriguingly, we found the same pattern of PRR inhibition and epigenetic modifications in NIKSmcHPV18 and HeLa cells, indicating that the evasion strategies are put in place at early stages of cancer progression and maintained over time even when the virus is fully integrated into the human genome, as in the case of HeLa cells.

Frequent suppression of cGAS and STING expression has been indeed observed in many types of human cancer, suggesting that this pathway may play a major role in suppressing tumorigenesis, and that its selective inhibition may occur frequently in viral-induced cancers (71,72). In this regard, the cGAS-STING pathway is crucial in triggering a potent down-stream interferon response against cytosolic DNA often present in cancer cells (73). Thus, inhibition of this signaling pathway by HPV18 is consistent with a model whereby infected cells escape the attention of the immune surveillance system, acquire further genetic mutations and eventually become transformed. The observed inhibition of cGAS-STING signaling may also help clarify

552 why cells harboring hrHPV infection do replicate despite the activation of the DNA damage
553 response (DDR), which ordinarily arrests cellular replication also through activation of the innate
554 response (74).

555 Although RIG-I was originally identified as a crucial cytoplasmic PRR for the
556 recognition of many negative-strand RNA viruses, mounting evidence indicates that it also plays
557 a role in detecting several DNA viruses [e.g. Epstein-Barr virus (EBV), Kaposi sarcoma-
558 associated herpesvirus (KSHV), herpes simplex virus 1 (HSV-1), and adenoviruses], and in some
559 cases it can recognize RNA species generated by RNA polymerase III, thus explaining the
560 observed inhibition in HPV-infected cells reported here (32, 33, 75, 76).

561 In recent years, several intracellular DNA sensor candidates have been identified. Most of
562 them appear to function through the essential adaptor protein, STING (11, 14, 66, 67). Although
563 the functional relevance of some of these DNA sensors still needs to be fully established, cGAS
564 and IFI16 have been identified as *bona fide* intracellular viral DNA receptors (77). Here we
565 demonstrate that, in KCs stably maintaining episomal viral DNA, cGAS and STING expression
566 levels are very low and are not induced by poly(dA:dT). Thus, the lack of the universal adaptor
567 protein STING *per se* is sufficient to explain the absence of IFN induction during HPV infection,
568 even though which DNA sensor is engaged by HPV still remains to be defined. The IFI16
569 protein is a viral DNA sensor that could be a potential candidate for binding and recognition of
570 the HPV DNA (78). Unfortunately, and despite many efforts, we have failed to demonstrate any
571 IFI16-HPV DNA interaction (36 and unpublished personal data). However, we found that IFI16
572 is downregulated under basal conditions in HPV-positive cells as a mechanism to attenuate its
573 activity as either DNA sensor or restriction factor (79).

574 When we turned our attention to the down-stream transcriptional factors activated by the

cGAS-STING and RIG-I-MAVS pathways, we made a series of interesting observations that helped us further elucidate the complex modulation of these pathways during HPV infection. While IRF3 protein levels were only marginally decreased by the presence of HPV18, both IRF1 and, albeit to a lesser extent, IRF7 were reduced in NIKSmcHPV18 cells. Consistent with the reduced availability of the IRF1 and IRF7 proteins, their binding activities to the consensus binding sites present in both ß and ß1 IFN enhancers were significantly reduced. In HeLa cells, IRF7 protein expression was almost undetectable, and it was not induced by DNA ligands, while IRF1 protein expression levels were less affected. According to the notion that IRF7 is a crucial factor for IFN-ß production, the induction of IRF7 by DNA ligand was robust in NIKS cells, whereas it was strongly reduced and delayed in NIKSmcHPV18 cells and completely ablated in HeLa cells (80-82).

A partial limitation of our study is that we are not providing definitive mechanistic details underlying the defects in the innate antiviral system observed in HPV-positive cells. Further studies are therefore clearly needed to clarify, for example, how the oncoproteins E6 and E7 or other early genes contribute to this inhibition. Despite this limitation, one of the strengths of this study is represented by the establishment of a reliable cell model where KCs stably harbor the entire viral genome, thereby closely recapitulating persistent HPV infection. Of note, similar results were also obtained with HeLa cells, which are known to contain integrated HPV18 DNA. In addition, our findings provide valuable information about innate immunity in KCs, which is a process still poorly characterized despite the fundamental role played by these cells not only in providing a physical barrier against infection and environmental insults, but also in sensing viral pathogens, thereby initiating and shaping local immune responses.

Overall, our findings provide compelling evidence that HPV persistence in KCs leads to

598 the inhibition of not only type I IFN but also type III IFN production in response to DNA
599 ligands, and that this effect is mainly due to the suppression of cGAS-STING signaling. As
600 stated above, deregulation of STING signaling in cells with persistent hrHPV infection can
601 hamper DDR, thereby enabling infected cells to evade host immunosurveillance and eventually
602 become tumorigenic.

603 The fact that we employed HPV-infected cells harboring the entire genome could explain
604 some inconsistencies between our results and those of others. In this regard, Lau and co-workers
605 have recently shown that E7 binds and degrades STING, thereby antagonizing the cGAS-STING
606 DNA-sensing pathway (17). Our data imply that inhibition of STING activity occurs mainly at
607 the transcriptional rather than post-transcriptional level. However, based on our data, we cannot
608 rule out that both mechanisms might be involved.

609 In summary, a series of reports dating back to the first decade of the 2000s, clearly
610 documented that hrHPV can inhibit several ISG transcripts mainly through E6 and E7 (22, 58,
611 63-65). In this study, we provide new evidence that the inhibitory action of HPV18 also affects
612 some ISGs crucial for the innate antiviral response such as PRRs and IRFs. In addition,
613 production of both IFN-ϐ and IFN-ϙ1 in response to poly(dA:dT) transfection was also impaired
614 in CaSki cells harboring integrated HPV16 (data not shown) through inhibition of cGAS-STING
615 signaling. Thus, our findings indicate that hrHPV genotypes have evolved broad-spectrum
616 mechanisms that allow simultaneous depletion of multiple effectors of the innate immunity
617 network rather than single downstream effectors.

618 These novel mechanistic insights into HPV immune evasion are critical for understanding
619 how HPV can persistently infect steadily unreactive cells and promote cancer.
620

Acknowledgments

We would like to thank Mart Ustav, Estonian Biocenter-Tartu, for providing us the minicircle system for HPV18 genome generation and Marcello Arsura for critically reviewing the manuscript.

644 **References**

645 1. Doorbar, J., W. Quint, L. Banks, I.G. Bravo, M. Stoler, T.R. Broker, and M.A. Stanley. 2012.
646 The biology and life-cycle of human papillomaviruses. *Vaccine*. 30 Suppl 5:F55-70. doi:
647 10.1016/j.vaccine.2012.06.083

648

649 2. Galloway, D.A., and L.A. Laimins. 2015. Human papillomaviruses: shared and distinct
650 pathways for pathogenesis. *Curr Opin Virol*. 14: 87-92. doi: 10.1016/j.coviro.2015.09.001

651

652 3. Moody, C.A., and L.A. Laimins. 2010. Human papillomavirus oncoproteins: pathways to
653 transformation. *Nat Rev Cancer*. 10: 550ï 560. doi: 10.1038/nrc2886

654

655 4. McBride, A.A. 2017. Mechanisms and strategies of papillomavirus replication. *Biol Chem*. pii:
656 /j/bchm.ahead-of-print/hsz-2017-0113/hsz-2017-0113.xml. doi: 10.1515/hsz-2017-0113.

657

658 5. Stanley, M.A. 2012. Epithelial cell responses to infection with human papillomavirus. *Clin*
659 *Microbiol Rev*. 25(2): 215-22. doi: 10.1128/CMR.05028-11

660

661 6. Westrich, J.A., C.J. Warren, and D. Pyeon. 2016. Evasion of host immune defenses by human
662 papillomavirus. *Virus Res*. pii: S0168-1702(16)30562-7. doi: 10.1016/j.virusres.2016.11.023

663

664 7. Hong, S., and L.A. Laimins. 2016. Manipulation of the innate immune response by human
665 papillomaviruses. *Virus Res*. pii: S0168-1702(16)30700-6. doi: 10.1016/j.virusres.2016.11.004

666

667 8. Egawa, N., K. Egawa, H. Griffin, and J. Doorbar. 2015. Human Papillomaviruses; Epithelial
668 Tropisms, and the Development of Neoplasia. *Viruses.* 7(7): 3863-90. doi: 10.3390/v7072802
669
670 9. Groves, I.J., and N. Coleman. 2015. Pathogenesis of human papillomavirus-associated
671 mucosal disease. *J Pathol.* 235(4): 527-38. doi: 10.1002/path.4496
672
673 10. Hasan, U.A., E. Bates, F. Takeshita, A. Biliato, R. Accardi, V. Bouverd , M. Mansour, I.
674 Vincent, L. Gissmann, T. Iftner, M. Sideri, F. Stubenrauch, and M. Tommasino. 2007. TLR9
675 expression and function is abolished by the cervical cancer-associated human papillomavirus
676 type 16. *J Immunol.* 178: 3186ï 3197. doi: 10.4049/jimmunol.178.5.3186
677
678 11. Brubaker, S.W., K.S. Bonham, I. Zanoni, and J.C. Kagan. 2015. Innate immune pattern
679 recognition: a cell biological perspective. *Annu Rev Immunol.* 33:257-90. doi: 10.1146/annurev-
680 immunol-032414-112240
681
682 12. Kalali, B.N., G. Kollisch, J. Mages, T. Muller, S. Bauer, H. Wagner, J. Ring, R. Lang, M.
683 Mempel, and M. Ollert. 2008. Doublestranded RNA induces an antiviral defense status in
684 epidermal keratinocytes through TLR3-, PKR-, and MDA5/RIG-I-mediated differential
685 signaling. *J Immunol.* 181: 2694ï 2704. doi: 10.4049/jimmunol.181.4.2694
686
687 13. Christensen, M.H., and S.R. Paludan. 2017. Viral evasion of DNA-stimulated innate immune
688 responses. *Cell Mol Immunol.* 14(1): 4-13. doi: 10.1038/cmi.2016.06
689

690 14. Dempsey, A., and A.G. Bowie. 2015. Innate immune recognition of DNA: A recent history.
691 *Virology*. 479-480: 146-52. doi: 10.1016/j.virol.2015.03.013
692
693 15. Karim, R., C. Meyers, C. Backendorf, K. Ludigs, R. Offringa, G.J. van Ommen, C.J. Melief,
694 S.H. van der Burg, and J.M. Boer. 2011. Human papillomavirus deregulates the response of a
695 cellular network comprising of chemotactic and proinflammatory genes. *Plos One*. 6:e17848.
696 doi: 10.1371/journal.pone.0017848
697
698 16. Karim, R., B. Tummers, C. Meyers, J.L. Biryukov, S. Alam, C. Backendorf, V. Jha, R.
699 Offringa, G.J. van Ommen, C.J. Melief, D. Guardavaccaro, J.M. Boer, and S.H. van der Burg.
700 2013. Human papillomavirus (HPV) upregulates the cellular deubiquitinase UCHL1 to suppress
701 the keratinocyte's innate immune response. *PLoS Pathog*. 9(5): e1003384. doi:
702 10.1371/journal.ppat.1003384
703
704 17. Lau, L., E.E. Gray, R.L. Brunette, and D.B. Stetson. 2015. DNA tumor virus oncogenes
705 antagonize the cGAS-STING DNA-sensing pathway. *Science*. 350(6260): 568-71. doi:
706 10.1126/science.aab3291
707
708 18. Perea, S.E., P. Massimi, and L. Banks. 2000. Human papillomavirus type 16 E7 impairs the
709 activation of the interferon regulatory factor-1. *Int J Mol Med*. 5(6): 661-6. doi:
710 10.3892/ijmm.5.6.661
711
712 19. Ronco, L.V., A.Y. Karpova, M. Vidal, and P.M. Howley. 1998. Human papillomavirus 16

713 E6 oncoprotein binds to interferon regulatory factor-3 and inhibits its transcriptional activity.
714 *Genes Dev*. 12(13): 2061-72. doi: 10.1101/gad.12.13.2061
715
716 20. Bergot, A.S., N. Ford, G.R. Leggatt, J.W. Wells, I.H. Frazer, and M.A. Grimbaldeston. 2014.
717 HPV16-E7 expression in squamous epithelium creates a local immune suppressive environment
718 via CCL2- and CCL5- mediated recruitment of mast cells. *PLoS Pathog*. 10(10): e1004466. doi:
719 10.1371/journal.ppat.1004466
720
721 21. Park, J.S., E.J. Kim, H.J. Kwon, E.S. Hwang, S.E. Namkoong, and S.J. Um. 2000.
722 Inactivation of interferon regulatory factor-1 tumor suppressor protein by HPV E7 oncoprotein.
723 Implication for the E7-mediated immune evasion mechanism in cervical carcinogenesis. *J Biol*
724 *Chem*. 275(10): 6764-9. doi: 10.1074/jbc.275.10.6764
725
726 22. Reiser, J., J. Hurst, M. Voges, P. Krauss, P. Münch, T. Iftner, and F. Stubenrauch. 2011.
727 High-risk human papillomaviruses repress constitutive kappa interferon transcription via E6 to
728 prevent pathogen recognition receptor and antiviral-gene expression. *J Virol*. 85(21): 11372-80.
729 doi: 10.1128/JVI.05279-11
730
731 23. Randall, R.E., and S. Goodbourn. 2008. Interferons and viruses: an interplay between
732 induction, signalling, antiviral responses and virus countermeasures. *J Gen Virol*. 89: 1-47. doi:
733 10.1099/vir.0.83391-0
734
735 24. Haller, O., G. Kochs, and F. Weber. 2006. The interferon response circuit: induction and

736 suppression by pathogenic viruses. *Virology*. 344: 119-130. doi: 10.1016/j.virol.2005.09.024
737
738 25. Muller, U., U. Steinhoff, L.F. Reis, S. Hemmi, J. Pavlovic, R.M. Zinkernagel, and M. Aguet.
739 1994. Functional role of type I and type II interferons in antiviral defense. *Science*. 264: 1918-
740 1921. doi: 10.1126/science.8009221
741
742 26. Schoggins, J.W., S.J. Wilson, M. Panis, M.Y. Murphy, C.T. Jones, P. Bieniasz, and C.M.
743 Rice. 2011. A diverse range of gene products are effectors of the type I interferon antiviral
744 response. *Nature*. 472: 481-485. doi: 10.1038/nature09907
745
746 27. Kotenko, S.V., G. Gallagher, V.V. Baurin, A. Lewis-Antes, M. Shen, N.K. Shah, J.A.
747 Langer, F. Sheikh, H. Dickensheets, and R.P. Donnelly. 2003. IFN-lambdas mediate antiviral
748 protection through a distinct class II cytokine receptor complex. *Nat Immunol.* 4: 69-77. doi:
749 10.1038/ni875
750
751 28. Sommereyns, C., S. Paul, P. Staeheli, and T. Michiels. 2008. IFN-lambda (IFN-lambda) is
752 expressed in a tissue- dependent fashion and primarily acts on epithelial cells in vivo. *PLoS*
753 *Pathog*. 4: e1000017. doi: 10.1371/journal.ppat.1000017
754
755 29. Lazear, H.M., T.J. Nice, and M.S. Diamond. 2015. Interferon-ə: Immune Functions at
756 Barrier Surfaces and Beyond. *Immunity*. 43(1): 15-28. doi: 10.1016/j.immuni.2015.07.001
757

30. Allen-Hoffmann, B.L., S.J. Schlosser, C.A. Ivarie, C.A. Sattler, L.F. Meisner, and S.L. O'Connor. 2000. Normal growth and differentiation in a spontaneously immortalized near-diploid human keratinocyte cell line, NIKS. *J Invest Dermatol.* 114(3): 444-55. doi: 10.1046/j.1523-1747.2000.00869.x

31. Egawa, N., Q. Wang, H.M. Griffin, I. Murakami, D. Jackson, R. Mahmood, and J. Doorbar. 2017. HPV16 and 18 genome amplification show different E4-dependence, with 16E4 enhancing E1 nuclear accumulation and replicative efficiency via its cell cycle arrest and kinase activation functions. *PLoS Pathog*. 13(3): e1006282. doi: 10.1371/journal.ppat.1006282

32. Ablasser, A., F. Bauernfeind, G. Hartmann, E. Latz, K.A. Fitzgerald, and V. Hornung. 2009. RIG-I-dependent sensing of poly(dA:dT) through the induction of an RNA polymerase III-transcribed RNA intermediate. *Nat Immunol.* 10(10): 1065-72. doi: 10.1038/ni.1779

33. Thompson, M.R., S. Sharma, M. Atianand, S.B. Jensen, S. Carpenter, D.M. Knipe, K.A. Fitzgerald, and E.A. Kurt-Jones. 2014. Interferon ɔ-inducible protein (IFI) 16 transcriptionally regulates type I interferons and other interferon-stimulated genes and controls the interferon response to both DNA and RNA viruses. *J Biol Chem.* 289(34): 2 3568-81. doi: 10.1074/jbc.M114.554147

34. Li, X.D., J. Wu, D. Gao, H. Wang, L. Sun, and Z.J. Chen. 2013. Pivotal roles of cGAS-cGAMP signaling in antiviral defense and immune adjuvant effects. *Science.* 341(6152): 1390-4. doi: 10.1126/science.1244040

781

782 35. Oshiumi, H., M. Miyashita, M. Okamoto, Y. Morioka, M. Okabe, M. Matsumoto, and T.
783 Seya. 2015. DDX60 is involved in RIG-I-dependent and independent antiviral responses, and its
784 function is attenuated by virus-induced EGFR activation. *Cell Rep*. 11(8): 1193-207. doi:
785 10.1016/j.celrep.2015.04.047

786

787 36. Lo Cigno, I., M. De Andrea, C. Borgogna, S. Albertini, M.M. Landini, A. Peretti, K.E.
788 Johnson, B. Chandran, S. Landolfo, and M. Gariglio. 2015. The nuclear DNA sensor IFI16 acts
789 as a restriction factor for human papillomavirus replication through epigenetic modifications of
790 the viral promoters. *J Virol*. 89: 7506-7520. doi: 10.1128/JVI.00013-15

791

792 37. Reinson, T., M. Toots, M. Kadaja, R. Pipitch, M. Allik, E. Ustav, and M. Ustav. 2013.
793 Engagement of the ATR-dependent DNA damage response at the human papillomavirus 18
794 replication centers during the initial amplification. *J Virol*. 87: 951-964. doi: 10.1128/JVI.01943-
795 12

796

797 38. Wilson, R., and L.A. Laimins. 2005. Differentiation of HPV-containing cells using
798 organotypic ñraftò culture or methylcellulose. *Methods Mol. Med*. 119:157-169. doi: 10.1385/1-
799 59259-982-6:157

800

801 39. Gugliesi, F., M. Mondini, R. Ravera, A. Robotti, M. De Andrea, G. Gribaudo, M. Gariglio,
802 and S. Landolfo. 2005. Up-regulation of the interferon inducible IFI16 gene by oxidative stress
803 triggers p53 transcriptional activity in endothelial cells. *J Leukoc Biol*. 77: 820ï 829. doi: 10

804 .1189/jlb.0904507
805
806 40. Xing, J., L. Ni, S. Wang, K. Wang, R. Lin, and C. Zhenga. 2013. Herpes Simplex Virus 1-
807 Encoded Tegument Protein VP16 Abrogates the Production of Beta Interferon (IFN) by
808 Inhibiting NF-əB Activation and Blocking IFN Regulatory Factor 3 To Recruit Its Coactivator
809 CBP. *J Virol.* 87(17):9788-801. doi: 10.1128/JVI.01440-13
810
811 41. Borgogna, C., E. Zavattaro, M. De Andrea, H.M. Griffin, V. Dell'Oste, B. Azzimonti M.M.
812 Landini, W.L. Peh, H. Pfister, J. Doorbar, S. Landolfo, and M. Gariglio. 2012. Characterization
813 of beta papillomavirus E4 expression in tumours from Epidermodysplasia Verruciformis patients
814 and in experimental models. *Virology.* 423(2):195-204. doi: 10.1016/j.virol.2011.11.029
815
816 42. Orav, M., L. Henno, H. Isok-Paas, J. Geimanen, M. Ustav, and E. Ustav. 2013.
817 Recombination-dependent oligomerization of human papillomavirus genomes upon transient
818 DNA replication. *J Virol.* 7(22): 12051-68. doi: 10.1128/JVI.01798-13
819
820 43. Isaacson Wechsler, E., Q. Wang, I. Roberts, E. Pagliarulo, D. Jackson, C. Untersperger, N.
821 Coleman, H. Griffin, and J. Doorbar. 2012. Reconstruction of human papillomavirus type 16-
822 mediated early-stage neoplasia implicates E6/E7 deregulation and the loss of contact inhibition
823 in neoplastic progression. *J Virol.* 86(11): 6358-64. doi: 10.1128/JVI.07069-11
824
825 44. Meissner, J.D. 1999. Nucleotide sequences and further characterization of human
826 papillomavirus DNA present in the CaSki, SiHa and HeLa cervical carcinoma cell lines. J Gen

827 Virol. 80 (Pt 7): 1725-33. doi: 10.1099/0022-1317-80-7-1725
828
829 45. Rösl, F., E.M. Westphal, and H. zur Hausen. 1989. Chromatin structure and transcriptional
830 regulation of human papillomavirus type 18 DNA in HeLa cells. *Mol Carcinog.* 2(2): 72-80.
831 doi:10.1002/mc.2940020205
832
833 46. Nees, M., J.M. Geoghegan, T. Hyman, S. Frank, L. Miller, and C.D. Woodworth. 2001.
834 Papillomavirus type 16 oncogenes downregulate expression of interferon-responsive genes and
835 upregulate proliferation-associated and NF-kappaB-responsive genes in cervical keratinocytes. *J*
836 *Virol.* 75(9): 4283-96.
837
838 47. Da Costa, R.M., M.M. Bastos, R. Medeiros, and P.A. Oliveira. 2016. The NFəB Signaling
839 Pathway in Papillomavirus-induced Lesions: Friend or Foe? *Anticancer Res.* 36(5): 2073-83.
840 Review.
841
842 48. James, M.A., J.H. Lee, and A.J. Klingelhutz. 2006. Human papillomavirus type 16 E6
843 activates NFHB, induces cIAP2 expression and protects against apoptosis in a PDZ binding
844 motif-dependent manner. *J Virol.* 80: 5301-5307. doi: 10.1128/JVI.01942-05
845
846 49. Wang, Y., Q. Lian, B. Yang, S. Yan, H. Zhou, L. He, G. Lin, Z. Lian, Z. Jiang, and B. Sun.
847 2015. TRIM30Ŭ Is a Negative-Feedback Regulator of the Intracellular DNA and DNA Virus-
848 Triggered Response by Targeting STING. *PLoS Pathog.* 11(6): e1005012. doi:
849 10.1371/journal.ppat.1005012

50. Wu, J., L. Sun, X. Chen, F. Du, H. Shi, C. Chen, and Z.J. Chen. 2013. Cyclic GMP-AMP is an endogenous second messenger in innate immune signaling by cytosolic DNA. *Science.* 339(6121): 826-30. doi: 10.1126/science.1229963

51. Prantner, D., D.J. Perkins, W. Lai, M.S. Williams, S. Sharma, K.A. Fitzgerald, and S.N. Vogel. 2012. 5,6-Dimethylxanthenone-4-acetic acid (DMXAA) activates stimulator of interferon gene (STING)-dependent innate immune pathways and is regulated by mitochondrial membrane potential. *J Biol Chem*. 287(47): 39776-88. doi: 10.1074/jbc.M112.382986

52. Odendall, C., E. Dixit, F. Stavru, H. Bierne, K.M. Franz, A.F. Durbin, S. Boulant, L. Gehrke, P. Cossart, and J.C. Kagan. 2014. Diverse intracellular pathogens activate type III interferon expression from peroxisomes. *Nat Immunol*. 15(8): 717-26. doi: 10.1038/ni.2915

53. Ma, F., B. Li, Y. Yu, S.S. Iyer, M. Sun, and G. Cheng. 2015. Positive feedback regulation of type I interferon by the interferon-stimulated gene STING. *EMBO Rep*. 16(2): 202-12. doi: 10.15252/embr.201439366

54. Liu, Y., M.L. Goulet, A. Sze, S.B. Hadj, S.M. Belgnaoui, R.R. Lababidi, C. Zheng, J.H. Fritz, D. Olagnier D, and R. Lin. 2016. RIG-I-Mediated STING Upregulation Restricts Herpes Simplex Virus 1 Infection. *J Virol*. 29;90(20):9406-19. doi: 10.1128/JVI.00748-16

55. Hong, S., K.P. Mehta, and L.A. Laimins. 2011. Suppression of STAT-1 expression by human

873 papillomaviruses is necessary for differentiation-dependent genome amplification and plasmid
874 maintenance. *J Virol.* 85(18): 9486-94. doi: 10.1128/JVI.05007-11
875
876 56. Cicchini, L., J.A. Westrich, T. Xu, D.W. Vermeer, J.N. Berger, E.T. Clambey, D. Lee, J.I.
877 Song, P.F. Lambert, R.O. Greer, J.H. Lee, and D. Pyeon. 2016. Suppression of antitumor
878 immune responses by human papillomavirus through epigenetic downregulation of CXCL14.
879 *MBio.* 7(3). pii: e00270-16. doi: 10.1128/mBio.00270-16
880
881 57. Munger, K., and D.L. Jones. 2015. Human papillomavirus carcinogenesis: an identity crisis
882 in the retinoblastoma tumor suppressor pathway. *J Virol.* 89(9): 4708-11. doi:
883 10.1128/JVI.03486-14
884
885 58. Rincon-Orozco, B., G. Halec, S. Rosenberger, D. Muschik, I. Nindl, A. Bachmann, T.M.
886 Ritter, B. Dondog, R. Ly, F.X. Bosch, R. Zawatzky, and F. Rösl. 2009. Epigenetic silencing of
887 interferon-kappa in human papillomavirus type 16-positive cells. *Cancer Res.* 69(22): 8718-25.
888 doi: 10.1158/0008-5472.CAN-09-0550
889
890 59. McLaughlin-Drubin, M.E., C.P. Crum, and K. Münger. 2011. Human papillomavirus E7
891 oncoprotein induces KDM6A and KDM6B histone demethylase expression and causes
892 epigenetic reprogramming. *Proc Natl Acad Sci U S A.* 108(5): 2130-5. doi:
893 10.1073/pnas.1009933108
894

895 60. Boccardo, E., A.P. Lepique, and L.L. Villa. 2010. The role of inflammation in HPV
896 carcinogenesis. *Carcinogenesis.* 31(11):1905-12. doi: 10.1093/carcin/bgq176
897
898 61. Ishikawa, H., Z. Ma, and G.N. Barber. 2009. STING regulates intracellular DNA-mediated,
899 type I interferon-dependent innate immunity. *Nature.* 461(7265): 788-92. doi:
900 10.1038/nature08476
901
902 62. Deschamps, T., and M. Kalamvoki. 2017. Impaired STING Pathway in Human
903 Osteosarcoma U2OS Cells Contributes to the Growth of ICP0-Null Mutant Herpes Simplex
904 Virus. *J Virol.* 91(9). pii: e00006-17. doi: 10.1128/JVI.00006-17
905
906 63. Chang, Y.E., and L.A. Laimins. 2000. Microarray analysis identifies interferon-inducible
907 genes and Stat-1 as major transcriptional targets of human papillomavirus type 31. *J Virol.* 74(9):
908 4174-82.
909
910 64. Beglin, M., M. Melar-New, and L.A. Laimins. 2009. Human papillomaviruses and the
911 interferon response. *J Interferon Cytokine Res.* 29(9): 629-35. doi: 10.1089/jir.2009.0075
912
913 65. Karstensen, B., S. Poppelreuther, M. Bonin, M. Walter, T. Iftner, and F. Stubenrauch. 2006.
914 Gene expression profiles reveal an upregulation of E2F and downregulation of interferon targets
915 by HPV18 but no changes between keratinocytes with integrated or episomal viral genomes.
916 *Virology.* 353(1): 200-9. doi: 10.1016/j.virol.2006.05.030
917

66. Knipe, D.M.. 2015. Nuclear sensing of viral DNA, epigenetic regulation of herpes simplex virus infection, and innate immunity. *Virology*. 479-480:153-9. doi: 10.1016/j.virol.2015.02.009

67. Chiang, C., and M.U. Gack. 2017. Post-translational control of intracellular pathogen sensing pathways. *Trends Immunol*. 38(1): 39-52. doi: 10.1016/j.it.2016.10.008

68. Chan, Y.K., and M.U. Gack. 2016.Viral evasion of intracellular DNA and RNA sensing. *Nat Rev Microbiol*. 14(6): 360-73. doi: 10.1038/nrmicro.2016.45

69. Ma, Z., and B. Damania. 2016. The cGAS-STING defense pathway and its counteraction by viruses. *Cell Host Microbe*. 19(2): 150-8. doi: 10.1016/j.chom.2016.01.010.

70. Gray, E., M.R. Pett, D. Ward, D.M. Winder, M.A. Stanley, I. Roberts, C.G. Scarpini, and N. Coleman. 2010. In vitro progression of human papillomavirus 16 episome-associated cervical neoplasia displays fundamental similarities to integrant-associated carcinogenesis. *Cancer Res.* 70(10): 4081-91. doi: 10.1158/0008-5472.CAN-09-3335

71. Ng, K.W., E.A. Marshall, J.C. Bell, and W.L. Lam. 2017. cGAS-STING and Cancer: Dichotomous Roles in Tumor Immunity and Development. *Trends Immunol*. pii:S1471-4906(17)30151-5. doi: 10.1016/j.it.2017.07.013.

939 72. Xia, T., H. Konno, J. Ahn, and G.N. Barber. 2016. Deregulation of STING Signaling in
940 Colorectal Carcinoma Constrains DNA Damage Responses and Correlates With Tumorigenesis.
941 *Cell Rep*. 14(2):282-97. doi:10.1016/j.celrep.2015.12.029.
942
943 73. Chatzinikolaou, G., I. Karakasilioti, and G.A. Garinis. 2014. DNA damage and innate
944 immunity: links and trade-offs. *Trends Immunol*. 35(9):429-35. doi:10.1016/j.it.2014.06.003.
945
946 74. Bristol, M.L., D. Das, and I.M. Morgan. 2017. Why Human Papillomaviruses Activate the
947 DNA Damage Response (DDR) and How Cellular and Viral Replication Persists in the Presence
948 of DDR Signaling. *Viruses*. 9(10). pii: E268. doi: 10.3390/v9100268. Review.
949
950 75. Rasmussen, S.B., S.B. Jensen, C. Nielsen, E. Quartin, H. Kato, Z.J. Chen, R.H. Silverman, S.
951 Akira, and S.R. Paludan. 2009. Herpes simplex virus infection is sensed by both Toll-like
952 receptors and retinoic acid-inducible gene- like receptors, which synergize to induce type I
953 interferon production. *J Gen Virol*. 90(Pt 1):74-8. doi: 10.1099/vir.0.005389-0
954
955 76. West, J.A., M. Wicks, S.M. Gregory, P. Chugh, S.R. Jacobs, Z. Zhang, K.M. Host, D.P.
956 Dittmer, and B. Damania. 2014. An important role for mitochondrial antiviral signaling protein
957 in the Kaposi's sarcoma-associated herpesvirus life cycle. *J Virol*. 88(10):5778-87. doi:
958 10.1128/JVI.03226-13
959

77. Luecke, S., and S.R. Paludan. 2016. Molecular requirements for sensing of intracellular microbial nucleic acids by the innate immune system. *Cytokine*. 98:4-14. doi: 10.1016/j.cyto.2016.10.003

78. Almine, J.F., C.A. O'Hare, G. Dunphy, I.R. Haga, R.J. Naik, A. Atrih, D.J. Connolly, J. Taylor, I.R., A.G. Bowie, P.M. Beard, and L. Unterholzner. 2017. IFI16 and cGAS cooperate in the activation of STING during DNA sensing in human keratinocytes. *Nat Commun*. 8:14392. doi: 10.1038/ncomms14392

79. Porter, S.S., W.H. Stepp, J.D. Stamos, and A.A. McBride. 2017. Host cell restriction factors that limit transcription and replication of human papillomavirus. *Virus Res.* 231:10-20. doi: 10.1016/j.virusres.2016.11.014

80. Sato, M., H. Suemori, N. Hata, M. Asagiri, K. Ogasawara, K. Nakao, T. Nakaya, M. Katsuki, S. Noguchi, N. Tanaka, and T. Taniguchi. 2000. Distinct and essential roles of transcription factors IRF-3 and IRF-7 in response to viruses for IFN-alpha/beta gene induction. *Immunity*. 13(4): 539-48. doi: 10.1016/S1074-7613(00)00053-4

81. Ning, S., J.S. Pagano, and G.N. Barber. 2011. IRF7: activation, regulation, modification and function. *Genes Immun*. 12(6): 399-414. doi: 10.1038/gene.2011.21

82. Honda, K., H. Yanai, H. Negishi, M. Asagiri, M. Sato, T. Mizutani, N. Shimada, Y. Ohba, A. Takaoka, N. Yoshida, and T. Taniguchi. 2005. IRF-7 is the master regulator of type-I interferon-dependent immune responses. *Nature*. 434(7034): 772-7. doi: 10.1038/nature03464

Grant Support

This work was supported by grants from the Italian Ministry for University and Research - MIUR (PRIN 2012 to CB), Compagnia di San Paolo (CSP2014 to CB), and Associazione Italiana per la Ricerca sul Cancro - AIRC Associazione Italiana per la Ricerca sul Cancro - AIRC (grants IG2012 and IG2016 to MG). The funders had no role in study design, data collection and interpretation, or the decision to submit the work for publication.

Disclosures:

The authors have no financial conflicts of interest.

Abbreviations: high-risk human papillomaviruses, hrHPVs; human papillomaviruses, HPVs; keratinocytes, KCs; pattern recognition receptor, PRR; near-diploid, spontaneously immortalized human keratinocyte cell line, NIKS; NIKS harboring multiple copies of episomal HPV18, NIKSmcHPV18; stimulator of interferon genes protein, STING; interferon regulatory factor, IRF; cyclic GMP-AMP synthase, cGAS; retinoic acid-inducible gene I, RIG-I; salmon sperm DNA, SS DNA; protonophore carbonyl cyanide m-chlorophenylhydrazone, CCCP; gamma-interferon-inducible protein 16, IFI16; mitochondrial antiviral-signaling protein, MAVS; glucuronidase beta, GUSB; fluorescent in situ hybridization, FISH; minichromosome mainteinance-7, MCM7; chromatin immunoprecipitation, ChIP; dimethylation of histone H3 lysine 4, H3K4me2; dimethylation of histone H3 lysine 9, H3K9me2; IFN-stimulated genes, ISGs; DNA damage response, DDR.

Figures Legends

FIGURE 1. Characterization of NIKSmcHPV18. (A) Total DNA extracts from NIKSmcHPV18 (lane 4 and 5) were prepared for Southern blot analysis. For all samples, genomic DNA (10 εg) was digested with either HindIII (lane 4) or EcoRI (lane 5)ð HPV18 minicircles do not have any HindIII restriction sites, while they contain one EcoRI site in the HPV genome and one in the linker, which give rise to two bands of 5,113 bp and 2,835 bp, respectively (lane 5). Standards of HPV18 minicircles digested with EcoRI corresponding to 10,000, 1,000, and 100 copies of the HPV18 genome per cell were included as internal control (lanes 1, 2, and 3, respectively). The 8,000-bp band corresponds to partially digested minicircle DNA. For detection of DNA, the filter was hybridized with a complete HPV18 genomic probe. (B) Phenotype of NIKSmcHPV18 cells in organotypic cultures. The images show histologic appearances following H&E staining, together with the expression of the cellular marker $p16^{INK4a}$ and MCM7, the viral protein E4, and the HPV18 genome as detected by fluorescent in situ hybridization (FISH), which was followed by DAPI counterstaining to visualize cell nuclei (blue). Scale bar=100 εm. (C) To measure viral replication, total cellular DNA was analyzed by qPCR after DpnI digestion in NIKSmcHPV18 cells at different passages. HPV18 levels were normalized to GAPDH levels. (D) qRT-PCR analysis of relative HPV18 early gene mRNA expression levels in NIKSmcHPV18 at different passages. Values were normalized to viral copy number and calculated using the following formula: mean relative mRNA expression ratio/mean relative HPV18 copy number. qPCR and qRT-PCR data are presented as mean values of biological triplicates. Error bars indicate SD.

FIGURE 2. HPV18 harboring cells fail to produce antiviral or pro-inflammatory cytokines. (A) Quantitative real-time PCR (qRT-PCR) analysis of mRNA expression levels in NIKS or

NIKSmcHPV18 grown as monolayer cultures. Values are normalized to GUSB mRNA, and plotted as fold induction over NIKS cells. Data are presented as mean values of biological triplicates. Error bars indicate SD *, P<0.05; **, P<0.01, ***P< 0.001; unpaired t test compared with NIKS monolayer. (B) qRT-PCR analysis of mRNA expression levels in NIKS or NIKSmcHPV18 organotypic raft cultures, cultured for 16 days at the air-liquid interface. Values were normalized to GUSB mRNA, and plotted as a fold induction over NIKS organotypic raft cultures. Data are presented as mean values of biological triplicates. Error bars indicate SD *P< 0.05, **P< 0.01, ***P< 0.001; unpaired t-test compared with NIKS organotypic raft cultures.

FIGURE 3. HPV18 impairs IFN-ϐ and IFN-ϑ1 production by DNA ligands. (A) qRT-PCR analysis of mRNA expression levels in NIKS, NIKSmcHPV18, and HeLa cells untransfected (white bars), mock-transfected (light grey bars), or transfected with either 1.25 ϵg poly(dA:dT) (black bars) or 1.25 ϵg SS DNA (dark grey bars) for 12 h. Values were normalized to GUSB mRNA, and plotted as a fold induction over mock-transfected NIKS cells. (B) ELISA quantitation of IFN-ϐ and IFN-ϑ1 protein in supernatants from cells transfected for 24 h as described in panel A. All qRT-PCR and ELISA data are presented as mean values of biological triplicates. Error bars indicate SD *P< 0.05, **P< 0.01, ***P< 0.001; unpaired t-test compared with NIKS cells untransfected, mock-transfected or transfected with either poly(dA:dT) or SS DNA. (C) Enzyme amplified sensitivity immunoassay (EASIA) quantification of IL-6 protein in supernatants from the cells transfected for 24 h as described in panel A. Data are presented as mean values of biological triplicates performed with cells between 20 and 30 passages. Error bars indicate SD *P< 0.05, **P< 0.01, ***P< 0.001; unpaired t-test compared with mock-transfected cells.

FIGURE 4. HPV18 disrupts different control points of the innate immune response in KCs. (A) Schematic model of the PRR pathways (B) Immunoblot analysis for cGAS, STING, RIG-I, MAVS, IFI16, and Ŭ-tubulin using total protein extracts from NIKS, NIKSmcHPV18, or HeLa cells following 24 h transfection in the absence (-) or presence (+) of 1.25 ɛg poly(dA:dT). (D) Immunoblot analysis for IRF1 and IRF7, (F) for IRF3 and (H) native gel analysis of IRF3 dimerization in total protein extracts from the cells described in A. (C, E, G and I). Densitometric analysis showing fold-change expression of the indicated proteins from three independent experiments. Error bars indicate SD *P< 0.05, **P< 0.01, ***P< 0.001; unpaired t-test compared with mock-transfected NIKS.

FIGURE 5. RIG-I delayed induction mediates the residual IFN-ɓ and IFN-ə1 production in HPV18 harboring cells. (A) qRT-PCR analysis of RIG-I mRNA expression levels in NIKS, NIKSmcHPV18, and HeLa cells mock-transfected or transfected with 1.25 ɛg poly(dA:dT) for the time points indicated. Values were normalized to GUSB mRNA, and plotted as fold induction over mock-transfected NIKS cells. qRT-PCR data are presented as mean values of biological triplicates. Error bars indicate SD *P< 0.05, **P< 0.01, ***P< 0.001; unpaired t-test compared with NIKS cells mock-transfected or transfected with either poly(dA:dT) for 3, 6, 12 or 24 h. (B) Immunoblot analysis for RIG-I expression levels in the cells described in panel A, and densitometric analysis showing fold-change expression from three independent experiments. Error bars indicate SD *P< 0.05, **P< 0.01, ***P< 0.001; unpaired t-test compared with mock-transfected NIKS.

(C) ELISA quantitation of IFN-ɓ and IFN-ə1 protein in supernatants from the cells described in

panel A. Data are presented as mean values of biological triplicates. Error bars indicate SD **P< 0.01, ***P< 0.001; one-way ANOVA followed by Bonferroniôs post test compared with NIKS cells mock-transfected. (D) ELISA quantitation of IFN-ß and IFN-ë1 protein in supernatants from NIKS, NIKSmcHPV18, and HeLa cells treated with 10 εM CCCP or vehicle alone (DMSO) for 30 min and then mock-transfected or transfected with 1.25 εg poly(dA:dT) for 24 h. Data are presented as mean values of biological triplicates. Error bars indicate SD *P< 0.05, **P< 0.01; unpaired t-test compared with vehicle-treated cells.

FIGURE 6. STAT1 mRNA is transcriptionally suppressed in HPV18 harboring cells. (A) qRT-PCR analysis of STAT1 mRNA expression levels. The values were normalized to GUSB mRNA, and plotted as a fold induction over mock-transfected NIKS cells. qRT-PCR data are presented as mean values of biological triplicates. Error bars indicate SD *P< 0.05, **P< 0.01, ***P< 0.001; unpaired t-test compared with NIKS cells mock-transfected or transfected with either poly(dA:dT) for 3, 6, 12 or 24 h. (B) Immunoblot analysis for STAT1 total and phosphorylated protein in NIKS, NIKSmcHPV18, and HeLa cells untransfected, mock-transfected or transfected with 1.25 εg poly(dA:dT) for the times indicated (left panel), and densitometric analysis showing fold-change expression from three independent experiments (right panel). Error bars indicate SD *P< 0.05, **P< 0.01, ***P< 0.001; unpaired t-test compared with mock-transfected NIKS (C) Immunoblot analysis of protein extracts from NIKS, NIKSmcHPV18, and HeLa cells treated with the proteasome inhibitor MG132 (30εM) for 8 h or vehicle alone (DMSO). All the Western blot data are representative of at least three experiments.

FIGURE 7. HPV18 promotes heterochromatin association at the promoter of STING, cGAS and

RIG-I genes. (A) Depiction of the promoter region from STING, cGAS, and RIG-I genes. Position of the primers used to assess the levels of histone binding at segment #1 and #2 is indicated, as well as that of the putative STAT1 and ISRE consensus sequence. (HPTMs: histone posttranslational modifications; bs: binding site; TSS: transcription start site). (B) Extracts were prepared from NIKS, NIKSmcHPV18, and HeLa cells. ChIP assay was carried out using antibodies specific to unmodified histone H3 (H3), dimethylated lysine 4 of H3 (H3K4me2), dimethylated lysine 9 of H3 (H3K9me2), or IgG as control. Immunoprecipitated promoter sequences were measured by qPCR, and CT values for the samples were equated to input CT values to give percent of input values for comparison. Values are representative of three independent experiments. Error bars indicate SD *P< 0.05, **P< 0.01; unpaired t-test compared with NIKS cells.

FIGURE 8. HPV18 impairs IRFs binding activity to the IRF element sequence. (A) Linear depiction of IFN-ß and IFN-α1 enhancer probes containing the IFN-regulatory factor element (IRFE). (B) ELISA-based analysis to assess IRF1, IRF3, and IRF7 binding activity in nuclear extracts (5 µg) from NIKS, NIKSmcHPV18, and HeLa cells mock-transfected or transfected with 1.25 µg poly(dA:dT) for the time points indicated. The probes described in panel A was used as capture probe, and anti-IRF1, anti-IRF7, and anti-IRF3 as detection antibodies. OD indicates optical density. The data are presented as mean values of biological triplicates for the IFN-ß enhancer. Error bars indicate SD *P< 0.05, **P< 0.01; one-way ANOVA followed by Bonferroni's post test compared with cells mock-transfected.

FIGURE 9. Schematic model of the innate immune response to poly(dA:dT) stimulation in NIKSmcHPV18 *vs*. NIKS cells. (TBK-1: TANK-binding kinase 1)

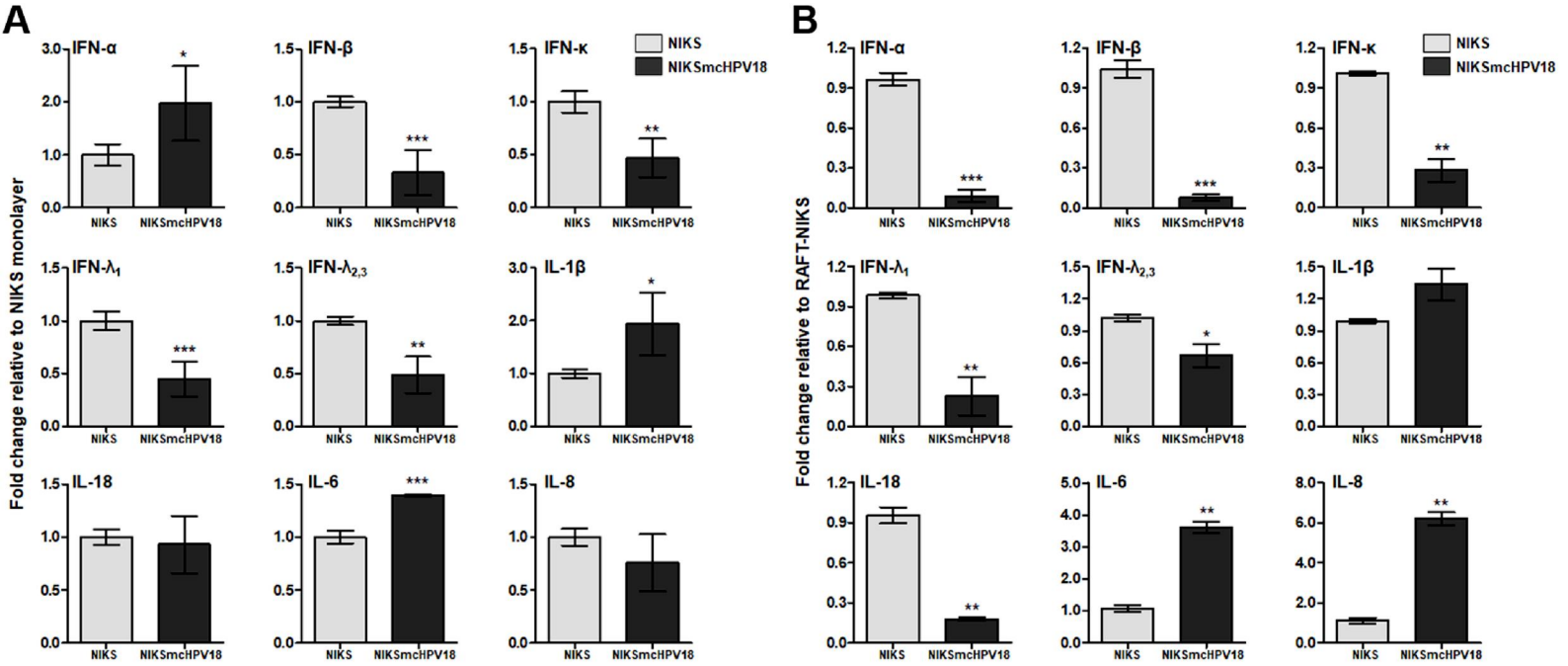
A
B
NIKS
NIKSmcHPV18
Fold change relative to NIKS monolayer
Fold change relative to RAFT-NIKS
IFN-α
IFN-β
IFN-κ
IFN-λ1
IFN-λ2,3
IL-1β
IL-18
IL-6
IL-8

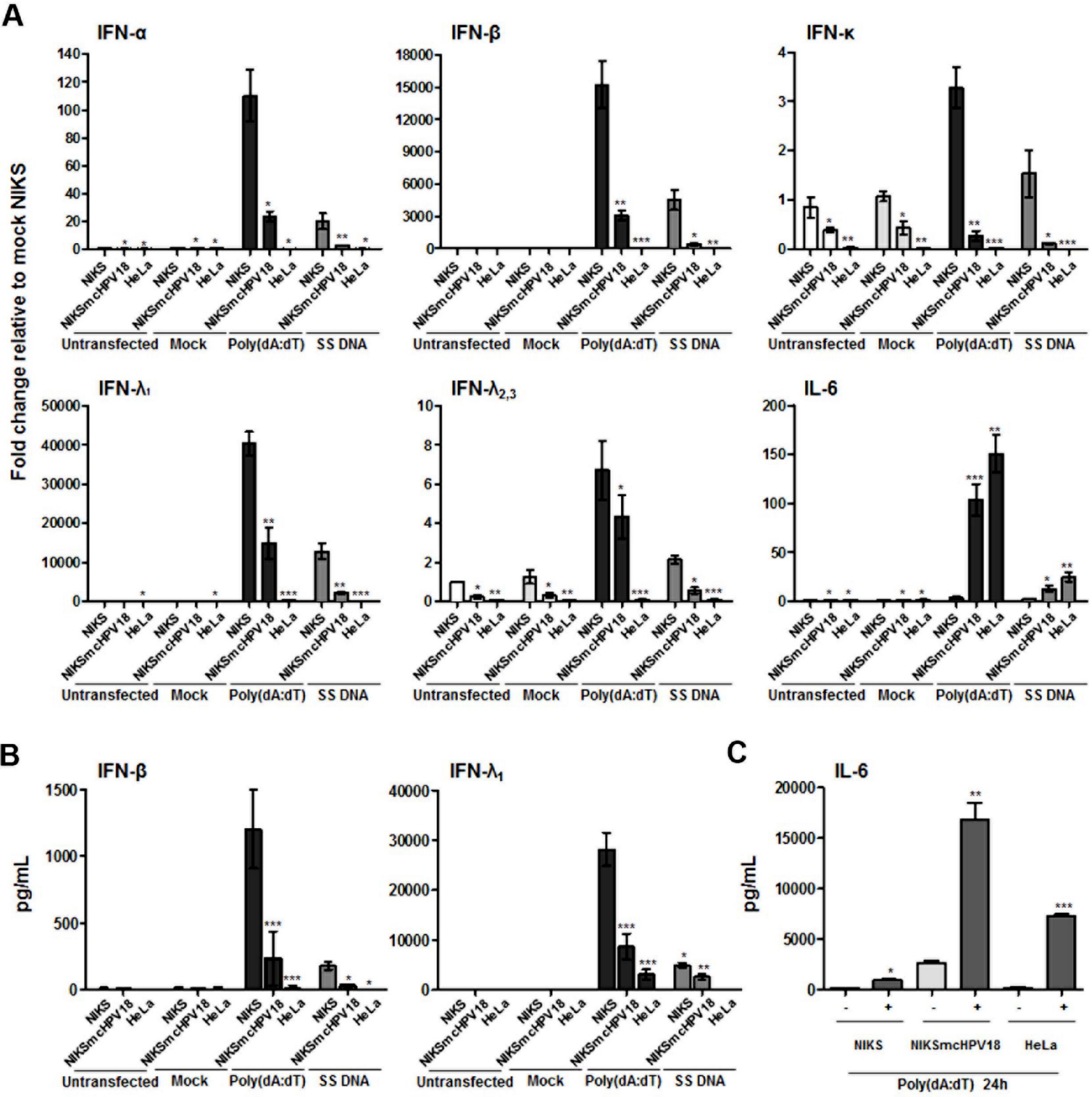
A
IFN-α
IFN-β
IFN-κ
IFN-λ1
IFN-λ2,3
IL-6
Fold change relative to mock NIKS
NIKS
NIKSmcHPV18
HeLa
Untransfected
Mock
Poly(dA:dT)
SS DNA
B
IFN-β
IFN-λ1
pg/mL
C
IL-6
pg/mL
Poly(dA:dT) 24h

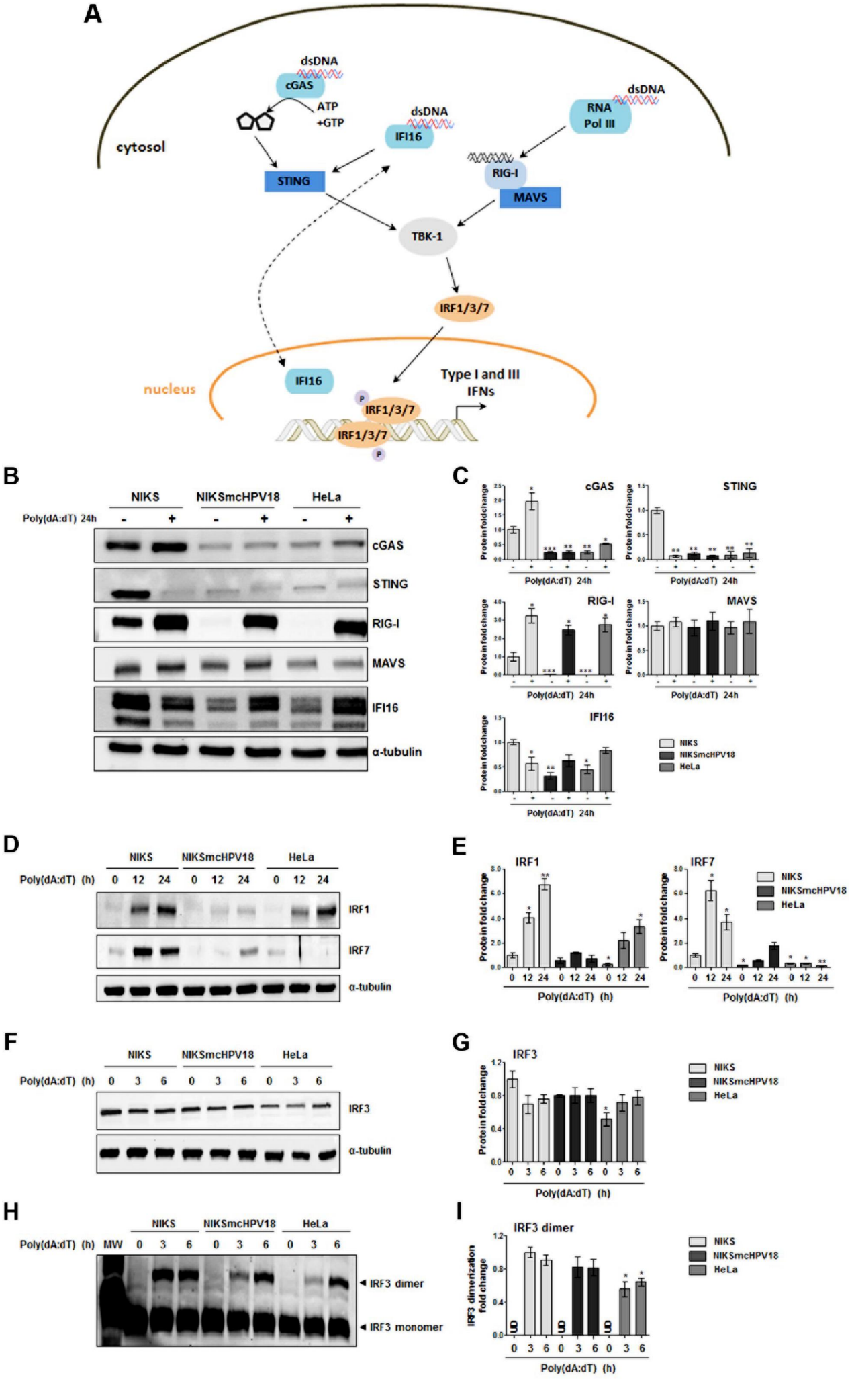
A
dsDNA
cGAS
ATP
+GTP
cytosol
dsDNA
IFI16
dsDNA
RNA
Pol III
STING
RIG-I
MAVS
TBK-1
IRF1/3/7
nucleus
IFI16
Type I and III
IFNs
IRF1/3/7
IRF1/3/7
B
NIKS
NIKSmcHPV18
HeLa
Poly(dA:dT) 24h
cGAS
STING
RIG-I
MAVS
IFI16
α-tubulin
C
cGAS
STING
RIG-I
MAVS
IFI16
Protein fold change
Poly(dA:dT) 24h
NIKS
NIKSmcHPV18
HeLa
D
NIKS
NIKSmcHPV18
HeLa
Poly(dA:dT) (h)
0 12 24 0 12 24 0 12 24
IRF1
IRF7
α-tubulin
E
IRF1
IRF7
Protein fold change
0 12 24 0 12 24 0 12 24
Poly(dA:dT) (h)
NIKS
NIKSmcHPV18
HeLa
F
NIKS
NIKSmcHPV18
HeLa
Poly(dA:dT) (h)
0 3 6 0 3 6 0 3 6
IRF3
α-tubulin
G
IRF3
Protein fold change
0 3 6 0 3 6 0 3 6
Poly(dA:dT) (h)
NIKS
NIKSmcHPV18
HeLa
H
NIKS
NIKSmcHPV18
HeLa
Poly(dA:dT) (h)
MW 0 3 6 0 3 6 0 3 6
IRF3 dimer
IRF3 monomer
I
IRF3 dimer
IRF3 dimerization fold change
0 3 6 0 3 6 0 3 6
Poly(dA:dT) (h)
NIKS
NIKSmcHPV18
HeLa

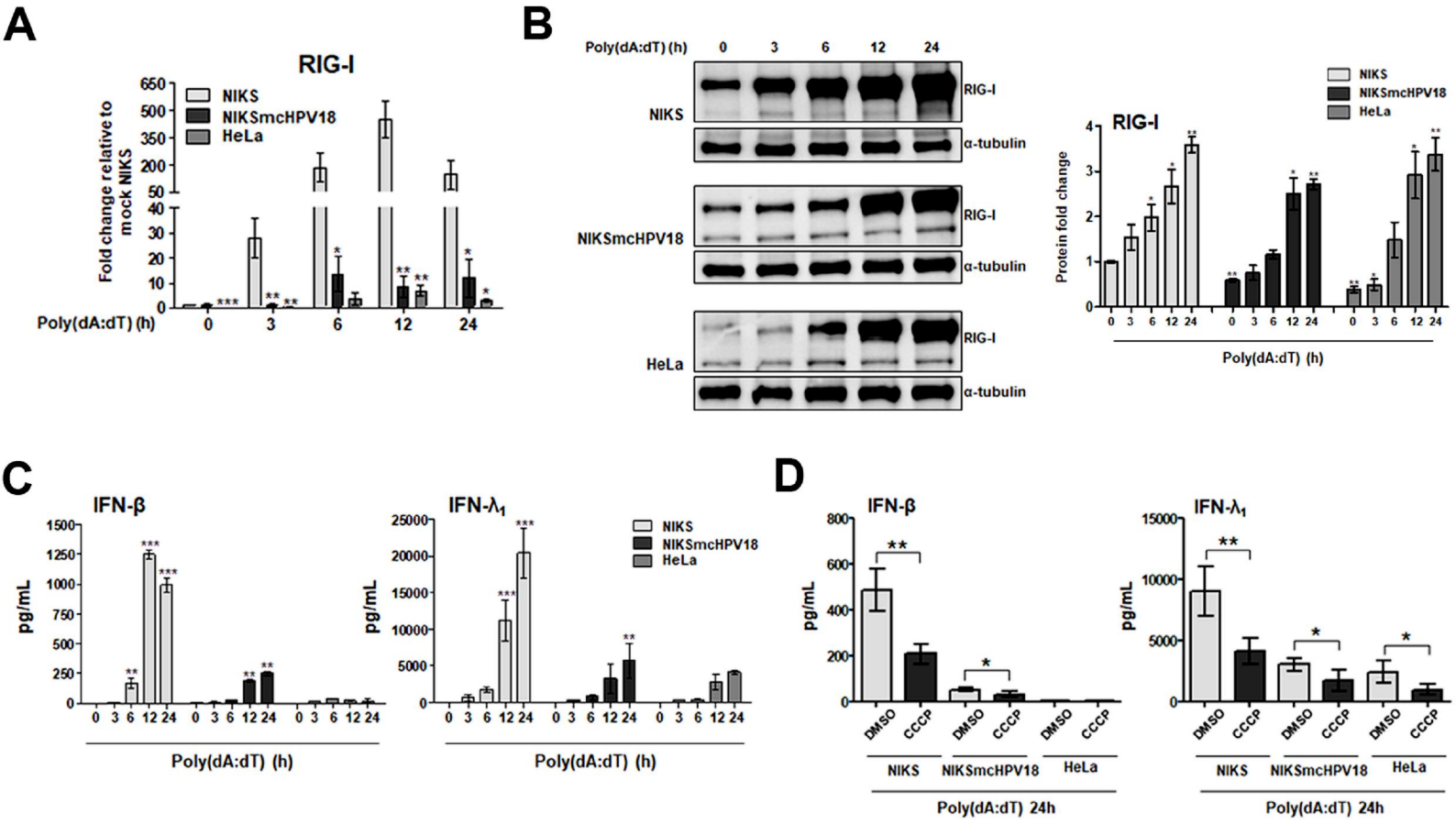
A
RIG-I
NIKS
NIKSmcHPV18
HeLa
Fold change relative to mock NIKS
Poly(dA:dT) (h)
B
Poly(dA:dT) (h)
RIG-I
α-tubulin
NIKS
NIKSmcHPV18
HeLa
Protein fold change
C
IFN-β
IFN-λ1
pg/mL
Poly(dA:dT) (h)
D
IFN-β
IFN-λ1
pg/mL
DMSO
CCCP
Poly(dA:dT) 24h

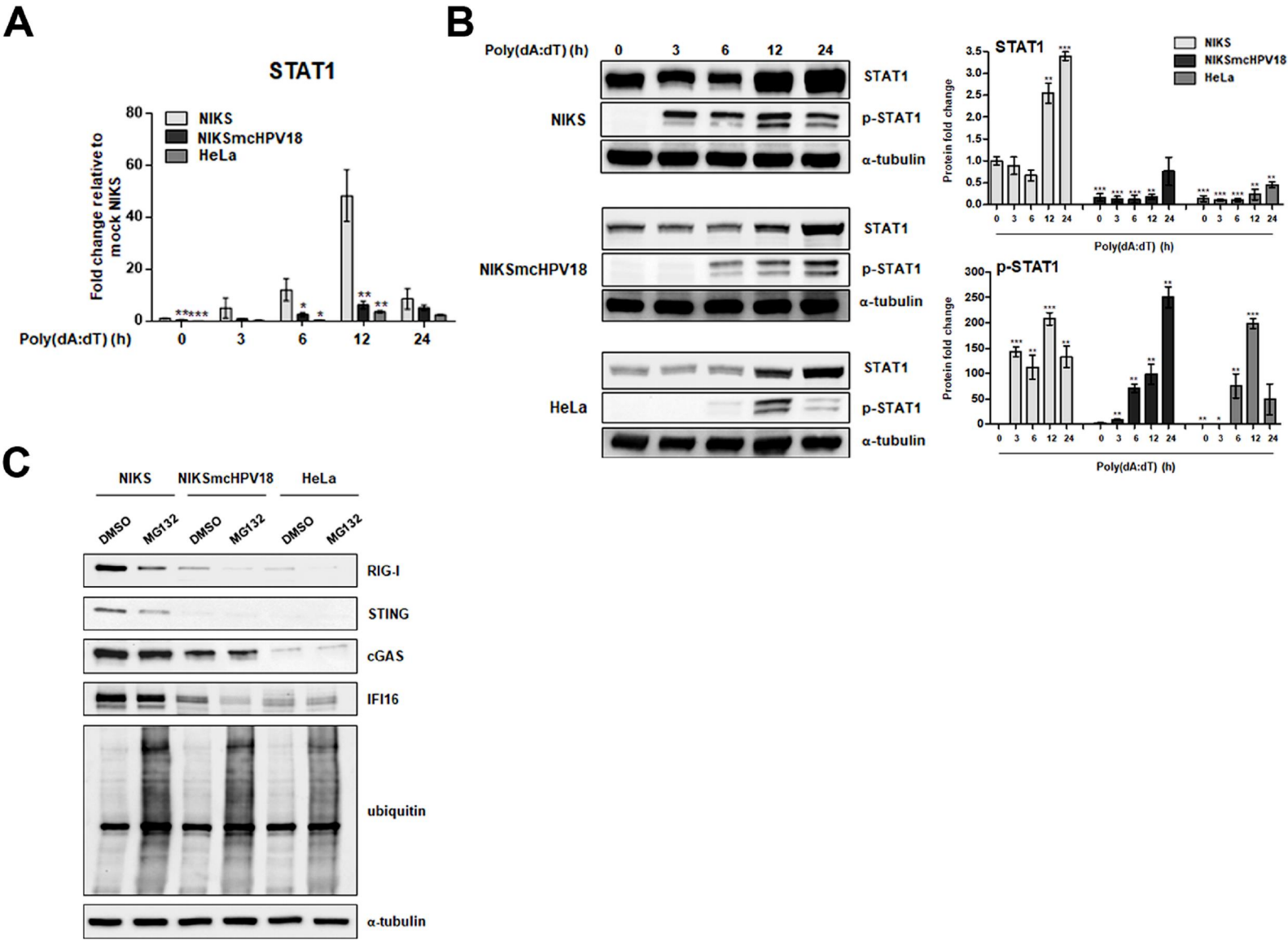
A
STAT1
NIKS
NIKSmcHPV18
HeLa
Fold change relative to mock NIKS
Poly(dA:dT) (h)
0
3
6
12
24
B
Poly(dA:dT) (h)
STAT1
p-STAT1
α-tubulin
NIKS
NIKSmcHPV18
HeLa
Protein fold change
C
DMSO
MG132
RIG-I
STING
cGAS
IFI16
ubiquitin
α-tubulin

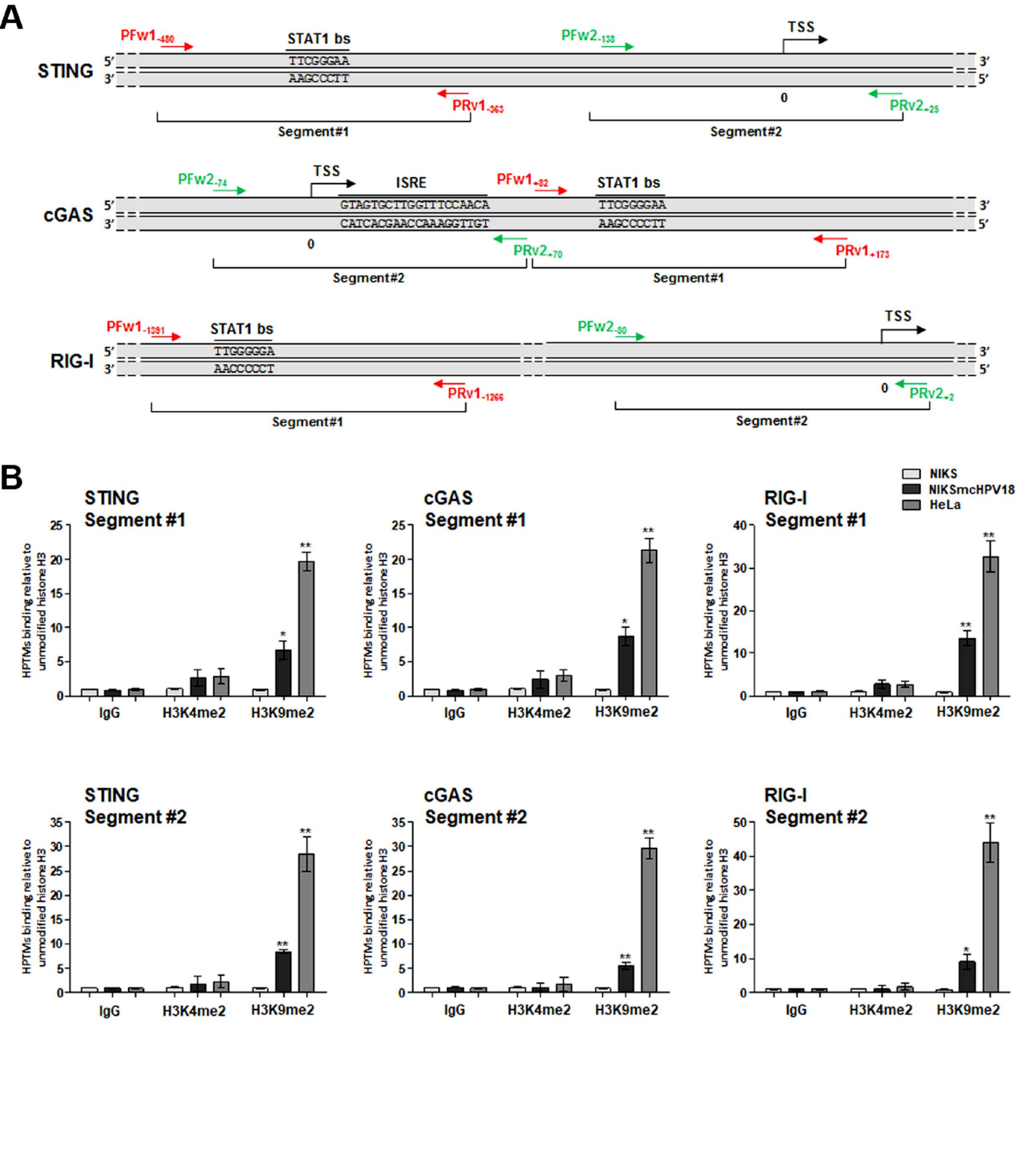
A
STING
PFw1-480
STAT1 bs
TTCGGGAA
AAGCCCTT
PFw2-138
TSS
PRv1-363
0
PRv2+25
Segment#1
Segment#2
cGAS
PFw2-74
TSS
ISRE
PFw1+82
STAT1 bs
GTAGTGCTTGGTTTCCAACA
CATCACGAACCAAAGGTTGT
TTCGGGGAA
AAGCCCCTT
0
PRv2+70
PRv1+173
Segment#2
Segment#1
RIG-I
PFw1-1391
STAT1 bs
TTGGGGGA
AACCCCCT
PFw2-50
TSS
PRv1-1266
0
PRv2+2
Segment#1
Segment#2
B
NIKS
NIKSmcHPV18
HeLa
STING
Segment #1
cGAS
Segment #1
RIG-I
Segment #1
STING
Segment #2
cGAS
Segment #2
RIG-I
Segment #2
HPTMs binding relative to unmodified histone H3
IgG
H3K4me2
H3K9me2

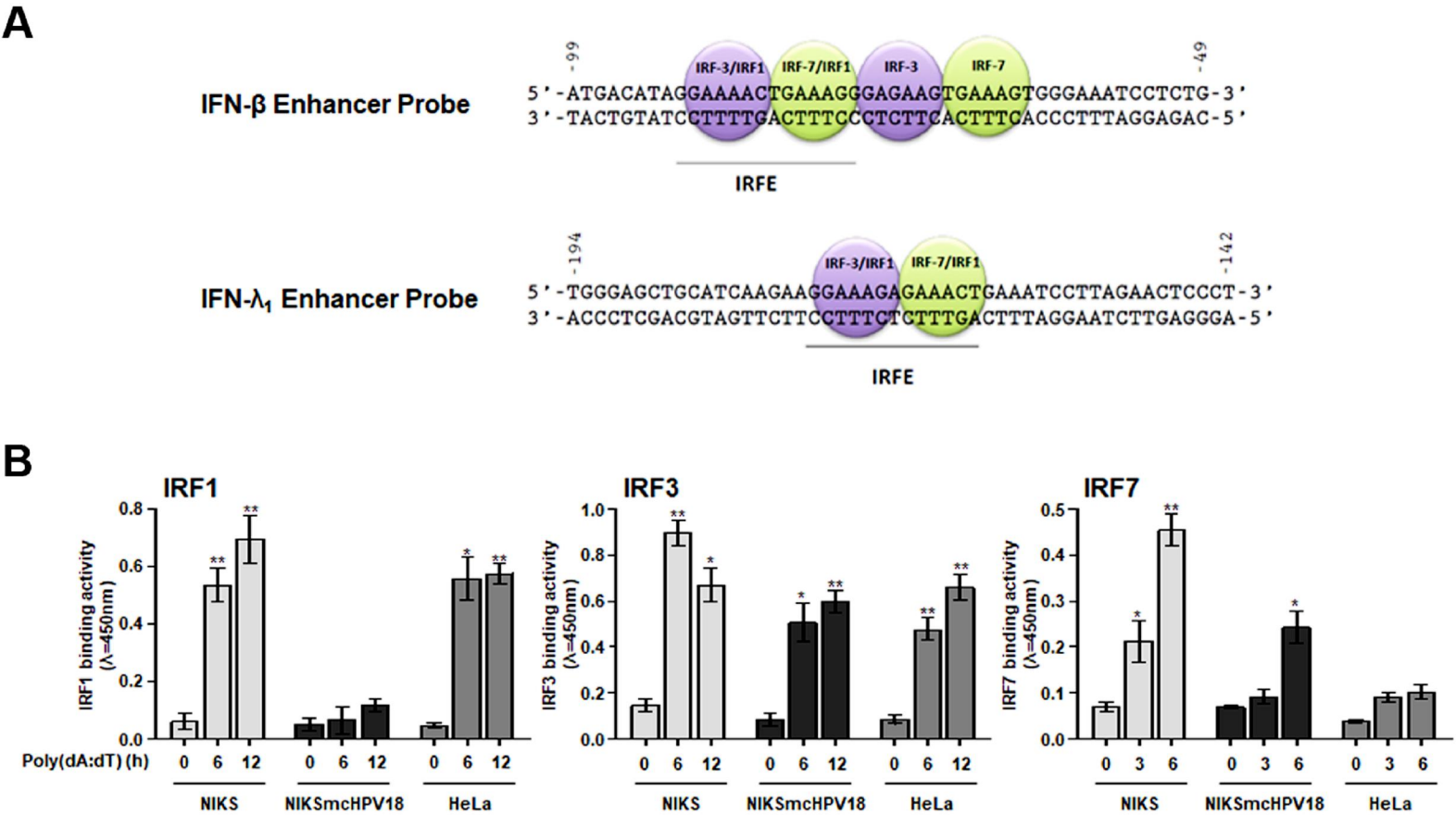
A
IFN-β Enhancer Probe
-99
-49
IRF-3/IRF1
IRF-7/IRF1
IRF-3
IRF-7
5'-ATGACATAGGAAAACTGAAAGGGAGAAGTGAAAGTGGGAAATCCTCTG-3'
3'-TACTGTATCCTTTTGACTTTCCCTCTTCACTTTCACCCTTTAGGAGAC-5'
IRFE
IFN-λ1 Enhancer Probe
-194
-142
IRF-3/IRF1
IRF-7/IRF1
5'-TGGGAGCTGCATCAAGAAGGAAAGAGAAACTGAAATCCTTAGAACTCCCT-3'
3'-ACCCTCGACGTAGTTCTTCCTTTCTCTTTGACTTTAGGAATCTTGAGGGA-5'
IRFE
B
IRF1
IRF3
IRF7
IRF1 binding activity (λ=450nm)
IRF3 binding activity (λ=450nm)
IRF7 binding activity (λ=450nm)
Poly(dA:dT) (h)
0 6 12
0 3 6
NIKS
NIKSmcHPV18
HeLa

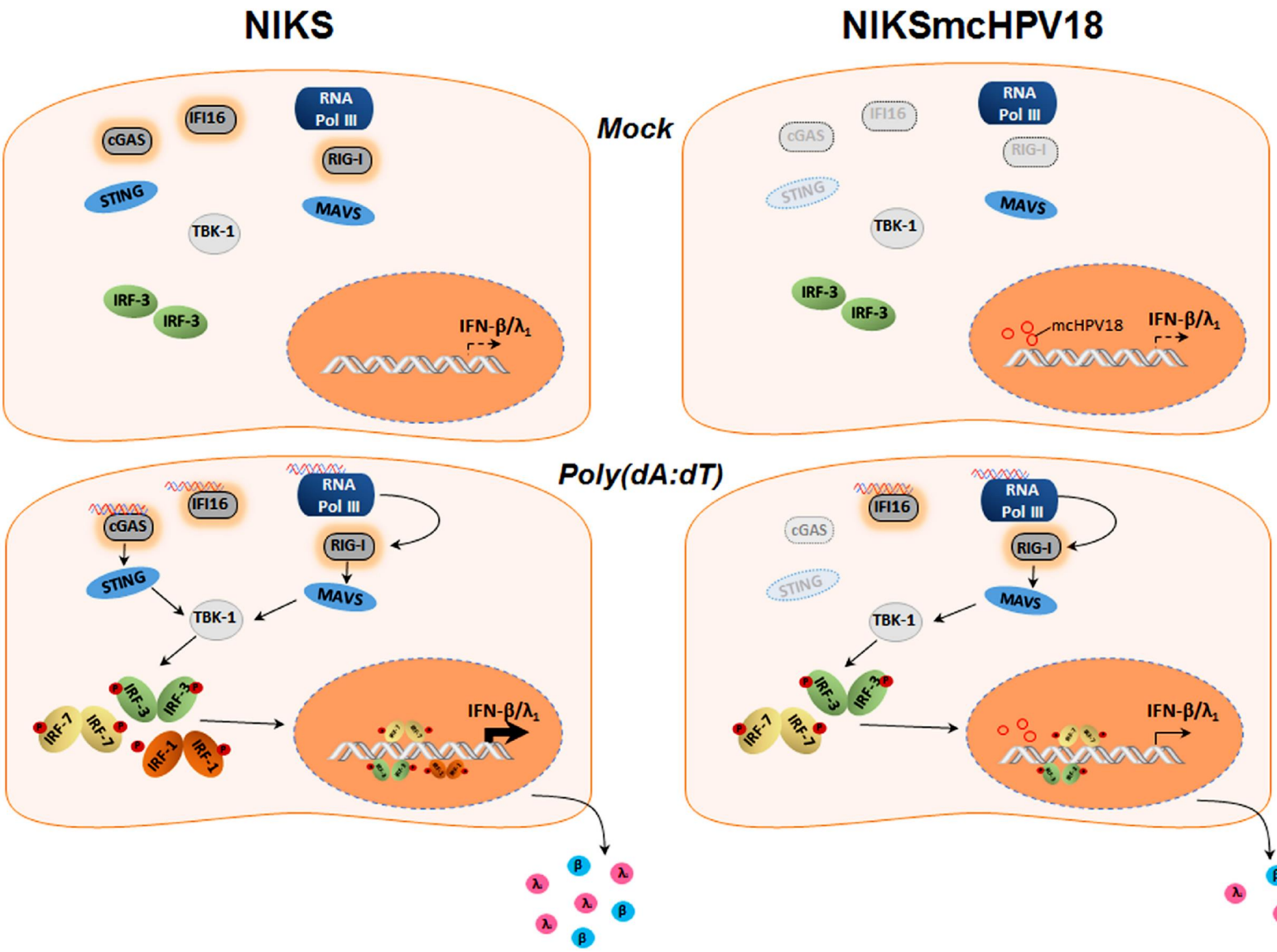
NIKS
NIKSmcHPV18
Mock
Poly(dA:dT)
cGAS
IFI16
RNA Pol III
RIG-I
STING
MAVS
TBK-1
IRF-3
IRF-7
IRF-1
mcHPV18
IFN-β/λ1